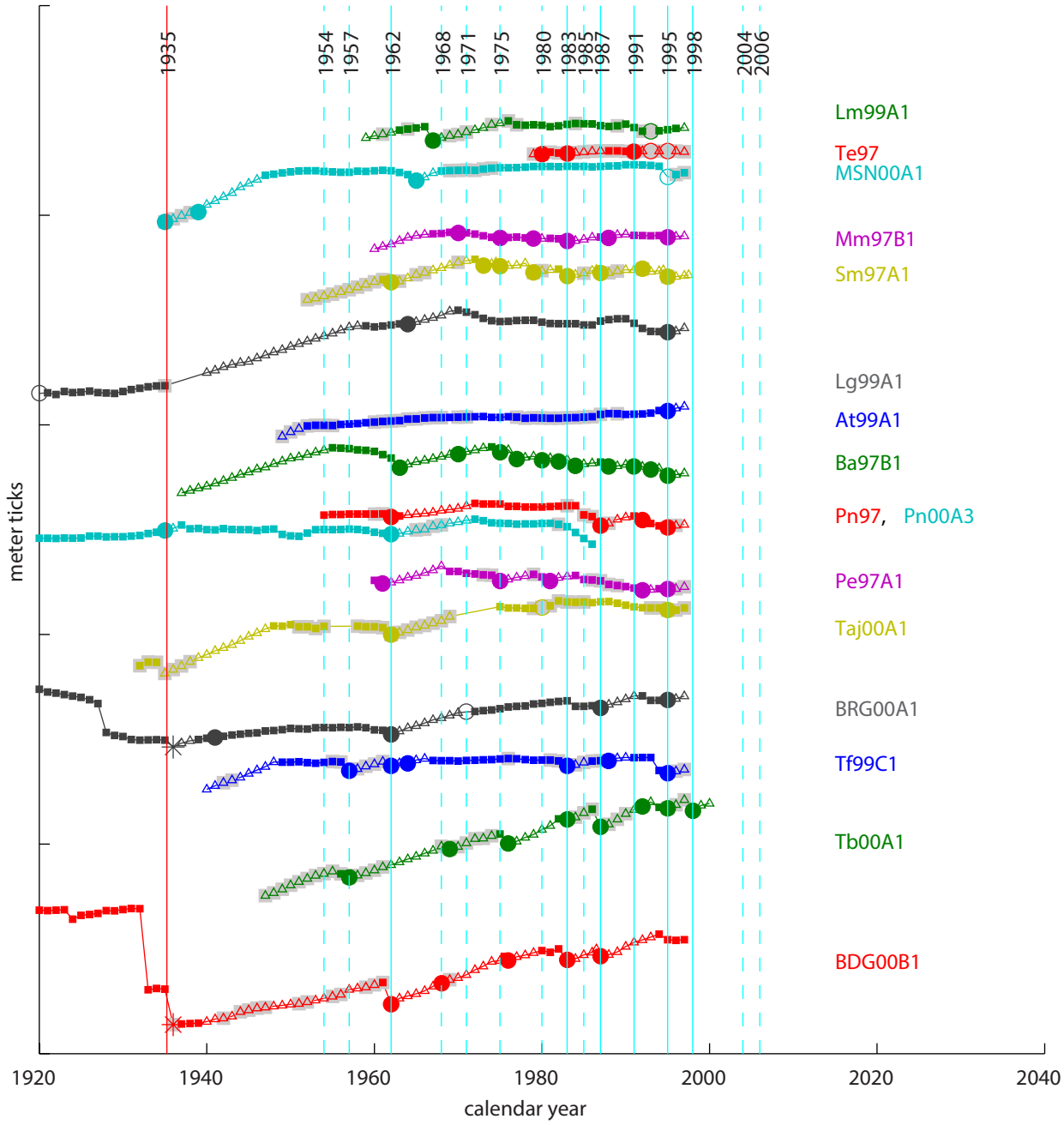

Figure S1A. Modern coral records from the Batu Islands, arranged from north to south with records from each site offset vertically from the last. Vertical blue lines mark likely (solid) and possible (dashed) regional oceanographic die-downs. Vertical red line marks the 1935 earthquake. Nearly all of these coral colonies died during the 1997–1998 IOD and algal bloom. Except for the southernmost site (Badgugu, BDG), we have no coral records in this region that are older than the late 19th century.

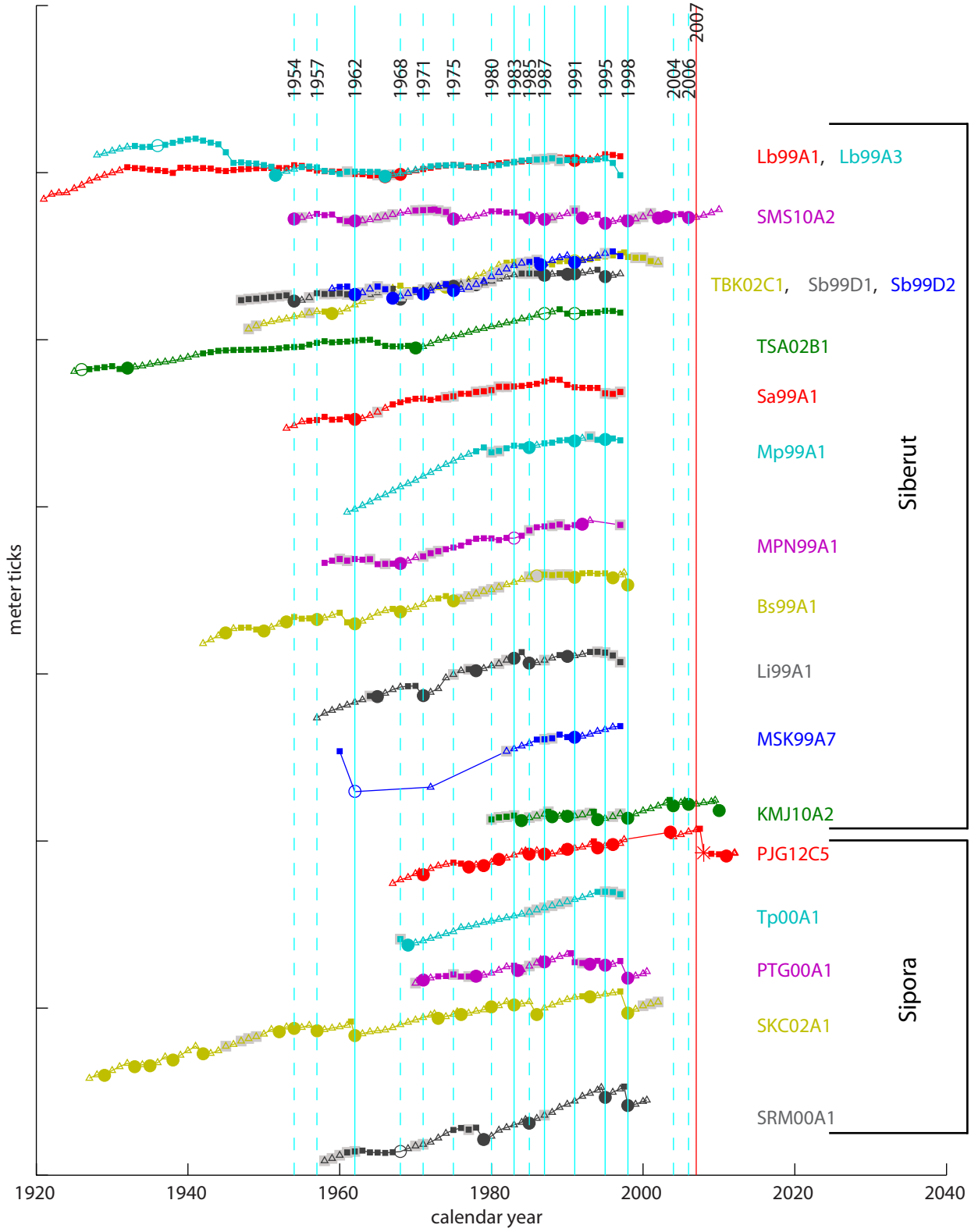

Figure S1B. Modern coral records from the Mentawai Islands arranged from northwest to southeast, offset as in Fig. S1A. Vertical blue lines mark likely (solid) and possible (dashed) regional oceanographic die-downs. Vertical red line marks the 2007 earthquake.

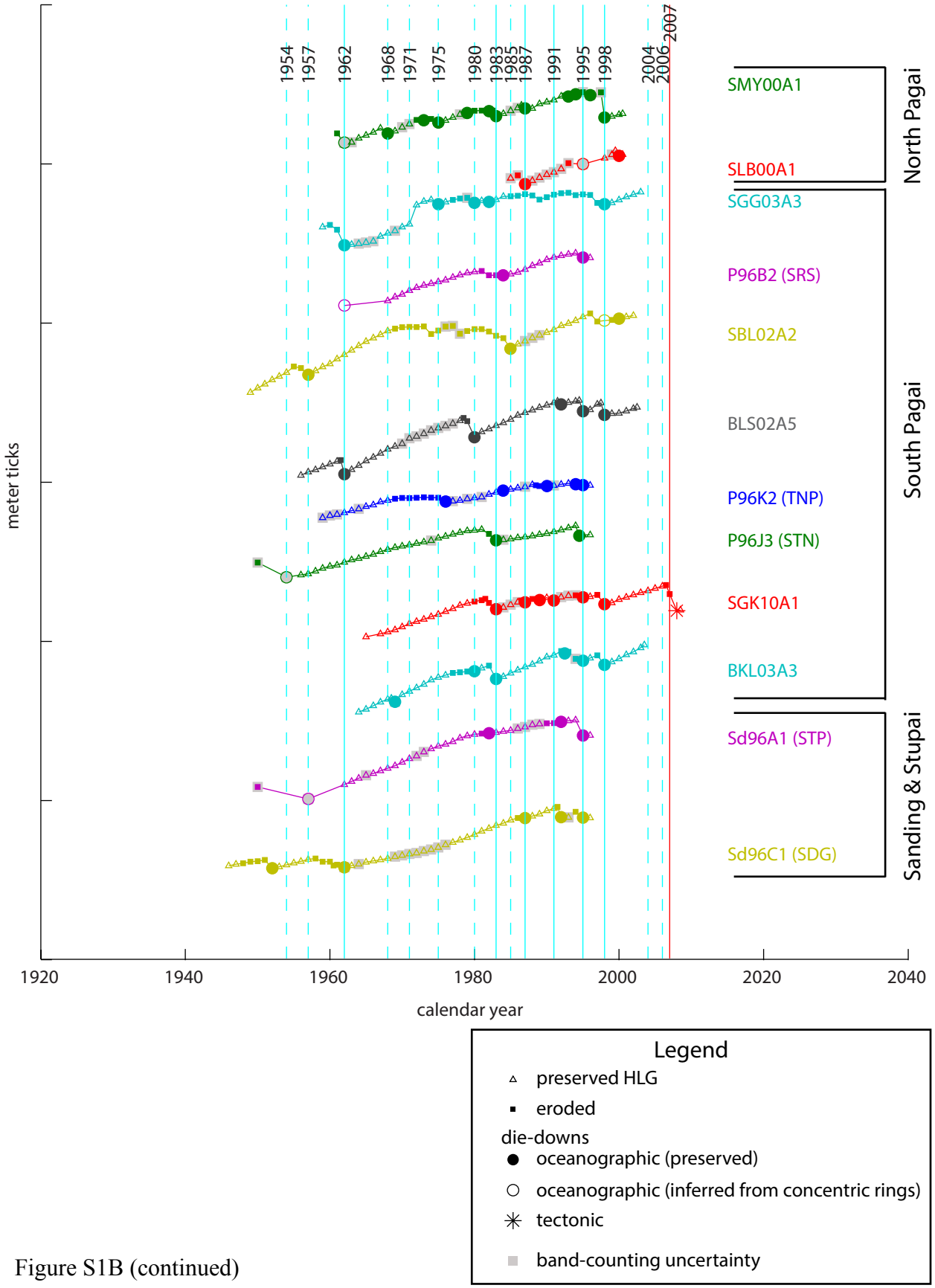

Figure S1B (continued)

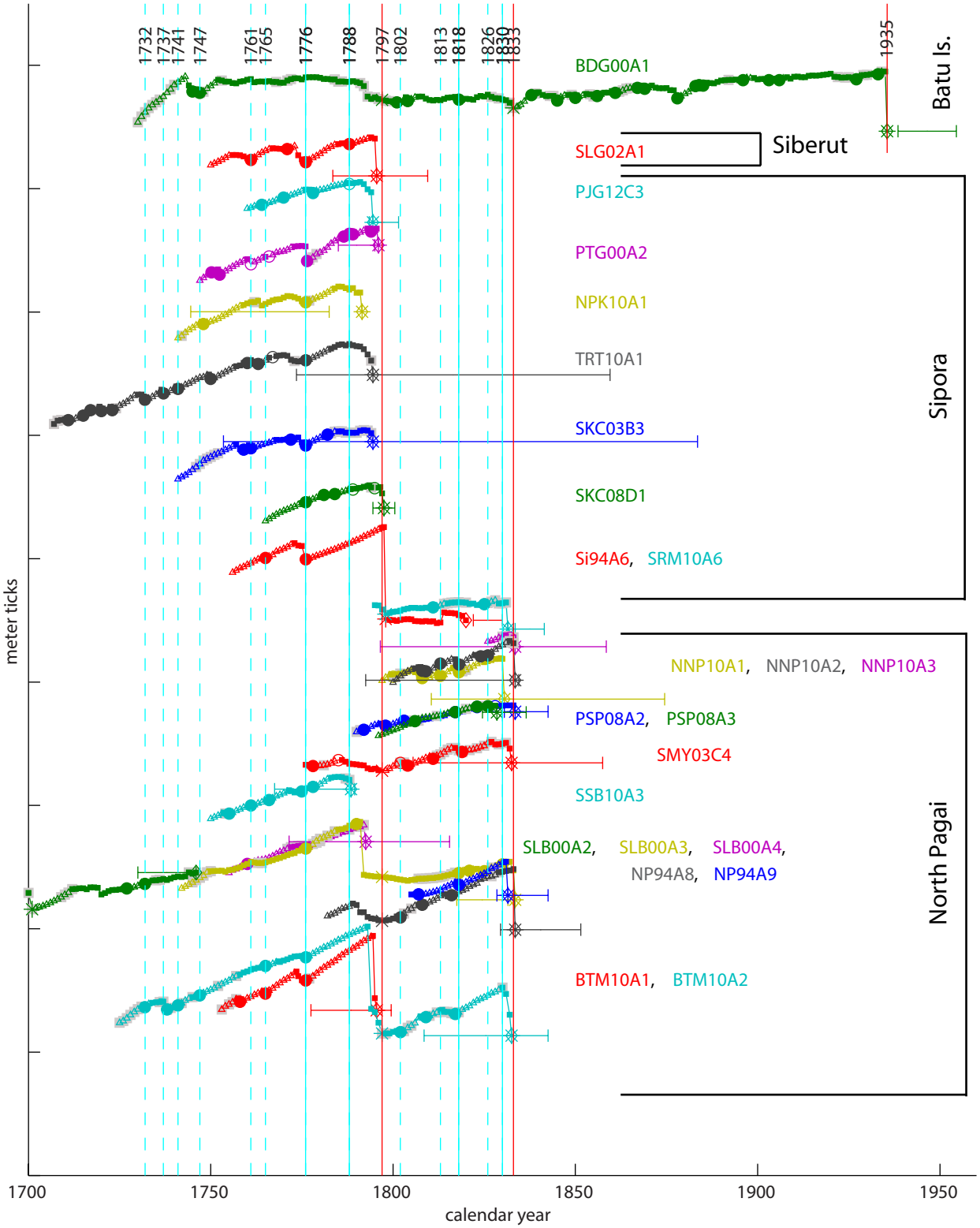

Figure S2. All 18th- and 19th-century coral records arranged from northwest to southeast with records from each site offset vertically from the last. All symbology as in Fig. S1 with the addition of a diamond symbol at the end of each record with error bars showing radiometric age uncertainty. Historical earthquakes are marked by red vertical lines.

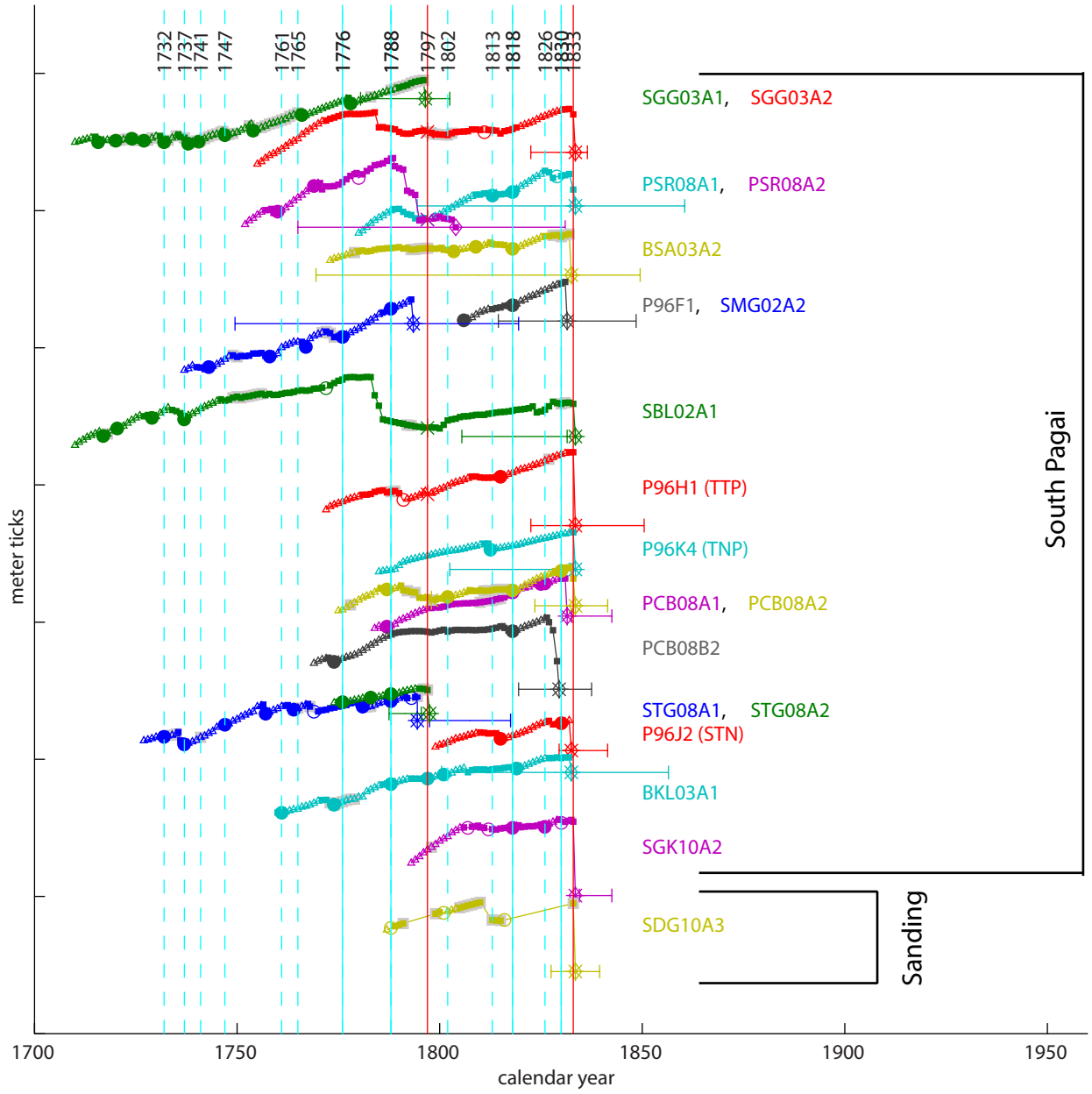

Figure S2. (continued)

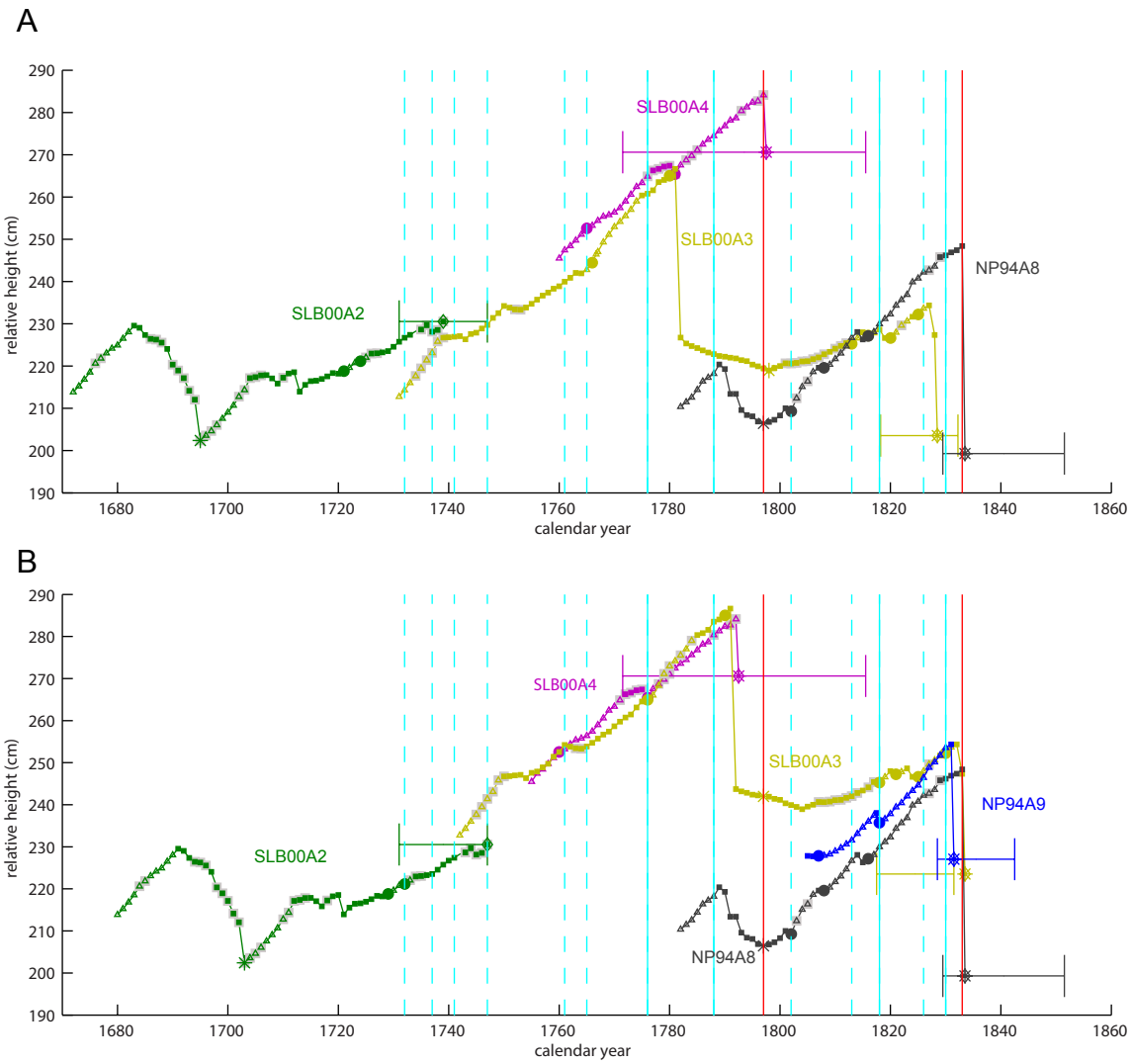

Figure S3. Modifications to interpretation of Silabu history (symbology as in Fig. S1-2).

A) Original interpretation from *Natawidjaja et al.* [2006]. There are conflicting growth histories after 1797: SLB00-A3 had moderate upward growth (~5 mm/yr) after 1797, whereas NP94-A8 and A9 both show very rapid upward growth (~12 mm/yr) during the same time period. It also seems unlikely that the surface that died in 1797 is completely un-eroded on A4 but eroded by 15 annual bands on A3, an interpretation espoused by Natawidjaja et al. to explain why the top of A3 was 20 cm lower than the top of A4.

B) New interpretation. We interpret that A3 and A4 both have about 5 bands eroded off the 1797 death surface, and that the top of A3 was originally the same elevation as the top of A4 but the head has since settled into the substrate. Restoring the A3 record 20 cm upward places it higher than A8 and A9. We hypothesize that A3 was preserved in a lagoon pool some 40 cm above the open ocean ELW in 1797, a plausible idea since A3 was much nearer to the beach than most of the other sampled corals. This explains why its upward growth was not tracking the 12 mm/yr of relative sea level rise recorded by A8 and A9. We use A3 and A4 to calculate the interseismic subsidence rate before 1797, but we use only A8 and A9 to calculate the rate between 1797 and 1833, since we have reason to believe A3 is not representative after 1797. We also use the elevation difference between A4 and A8 to calculate the 1797 coseismic uplift and ignore the smaller uplift suggested by the step in the A3 record, as did *Natawidjaja et al.* [2006].

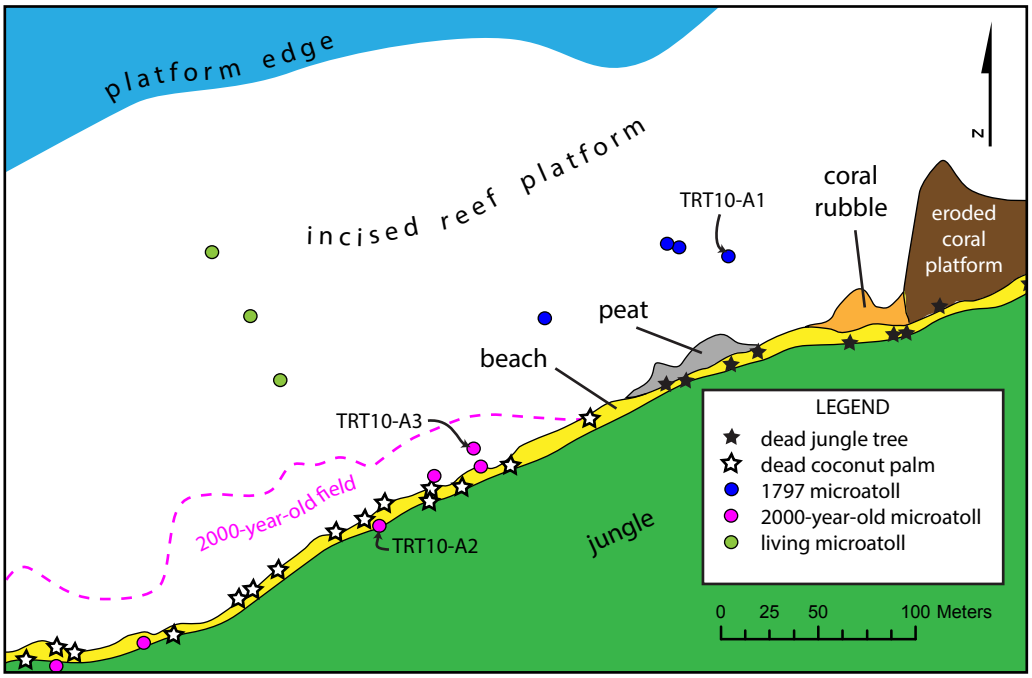

Figure S4. Map of the Trait site. Dead trees which line the beach are evidence of recent interseismic subsidence. In addition to a population of corals that died due to uplift in 1797, there is a large population of ~2000-year-old microatolls in and near the beach. Dates from TRT10-A2 and A3 were presented by *Philibosian et al.* [2012].

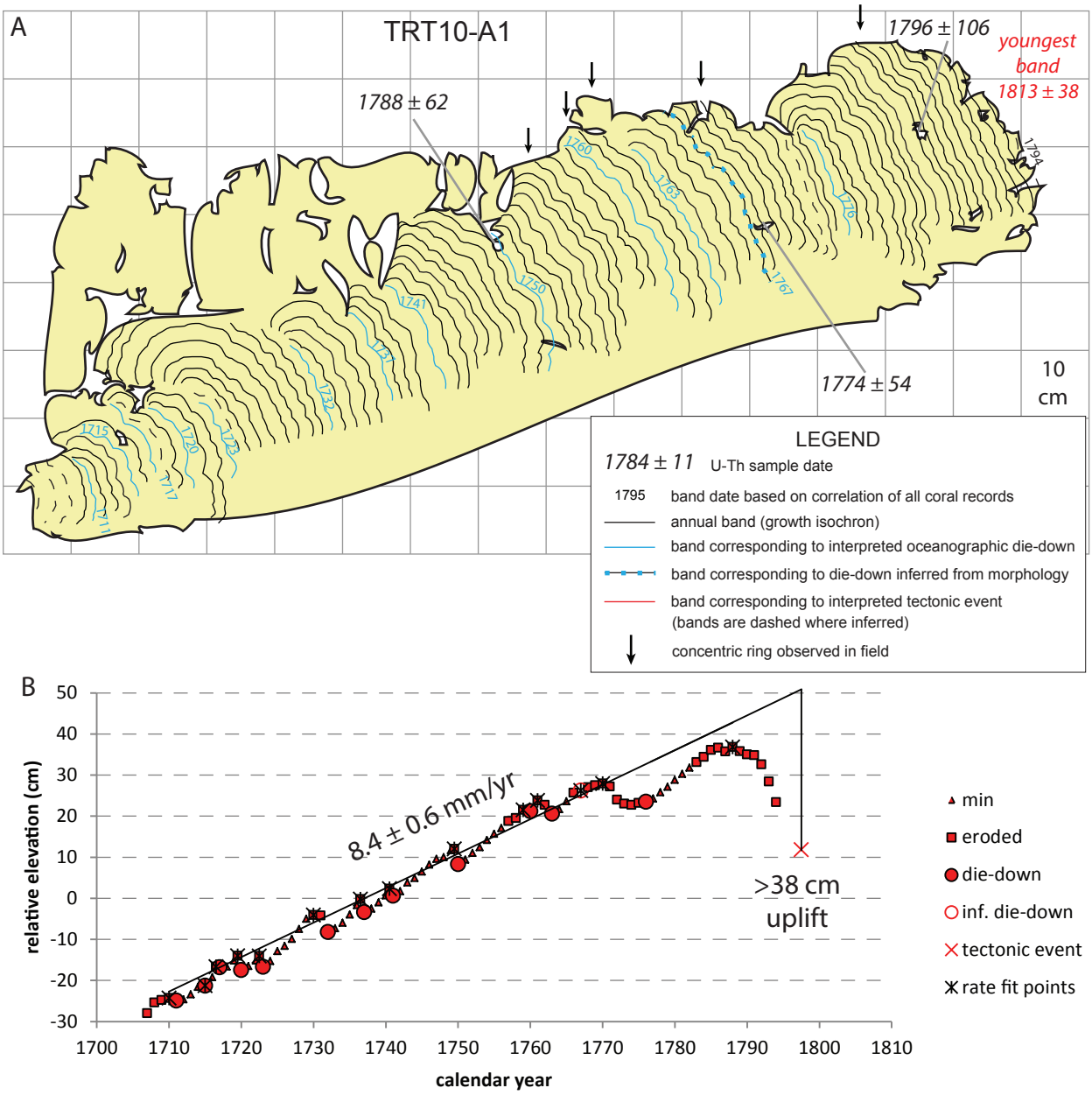

Figure S5. A) Cross section and B) growth history of TRT10-A1 from Trait. Youngest preserved band date in red is based on band counting and a weighted average of the U-Th dates. Some die-downs are not clearly preserved but can be inferred from the concentric ring morphology of the microatoll.

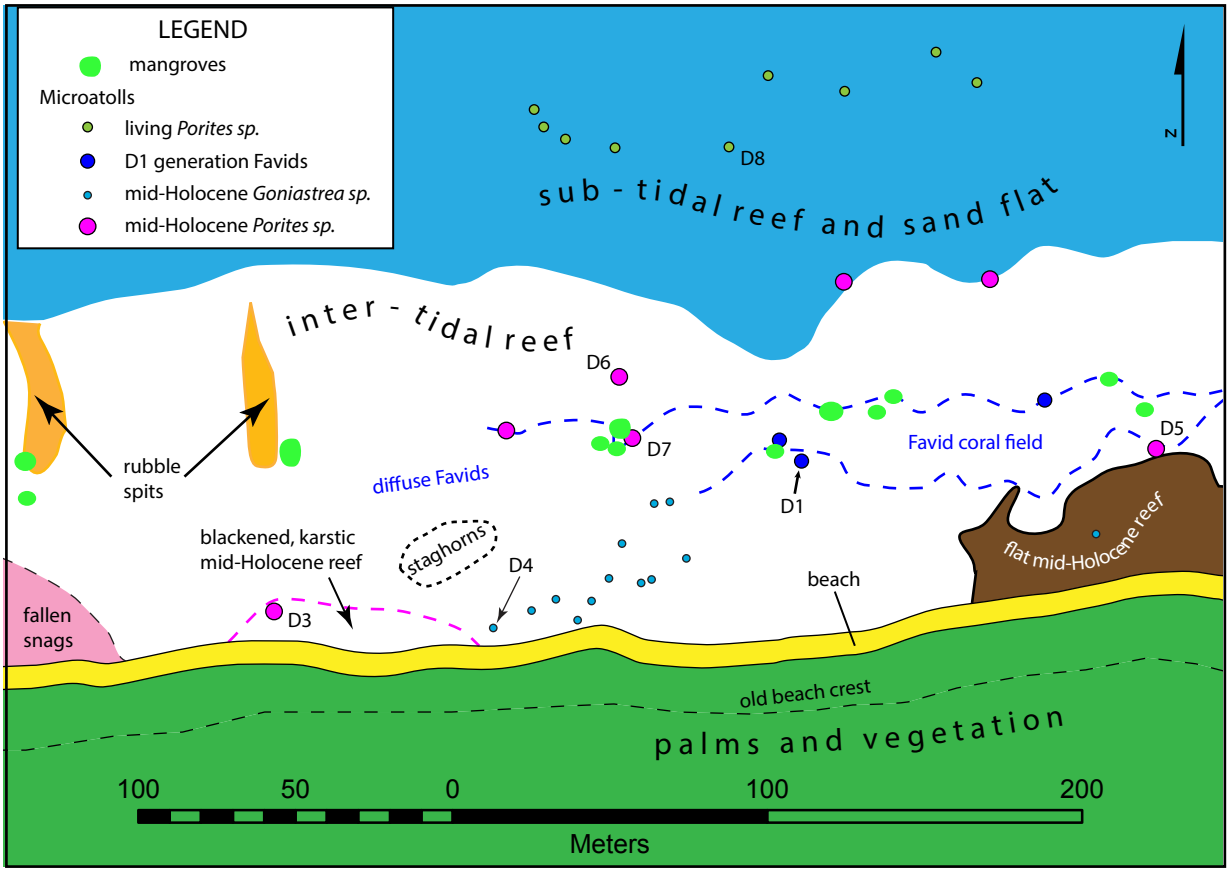

Figure S6. Map of Sikici site D. A large field of ~1-meter diameter Favid corals died due to uplift in the 1797 earthquake, based on analysis of the sampled slab SKC08-D1. Chiseled samples of heads D3-D7 date to the mid-Holocene and were presented by *Philibosian et al.* [2012].

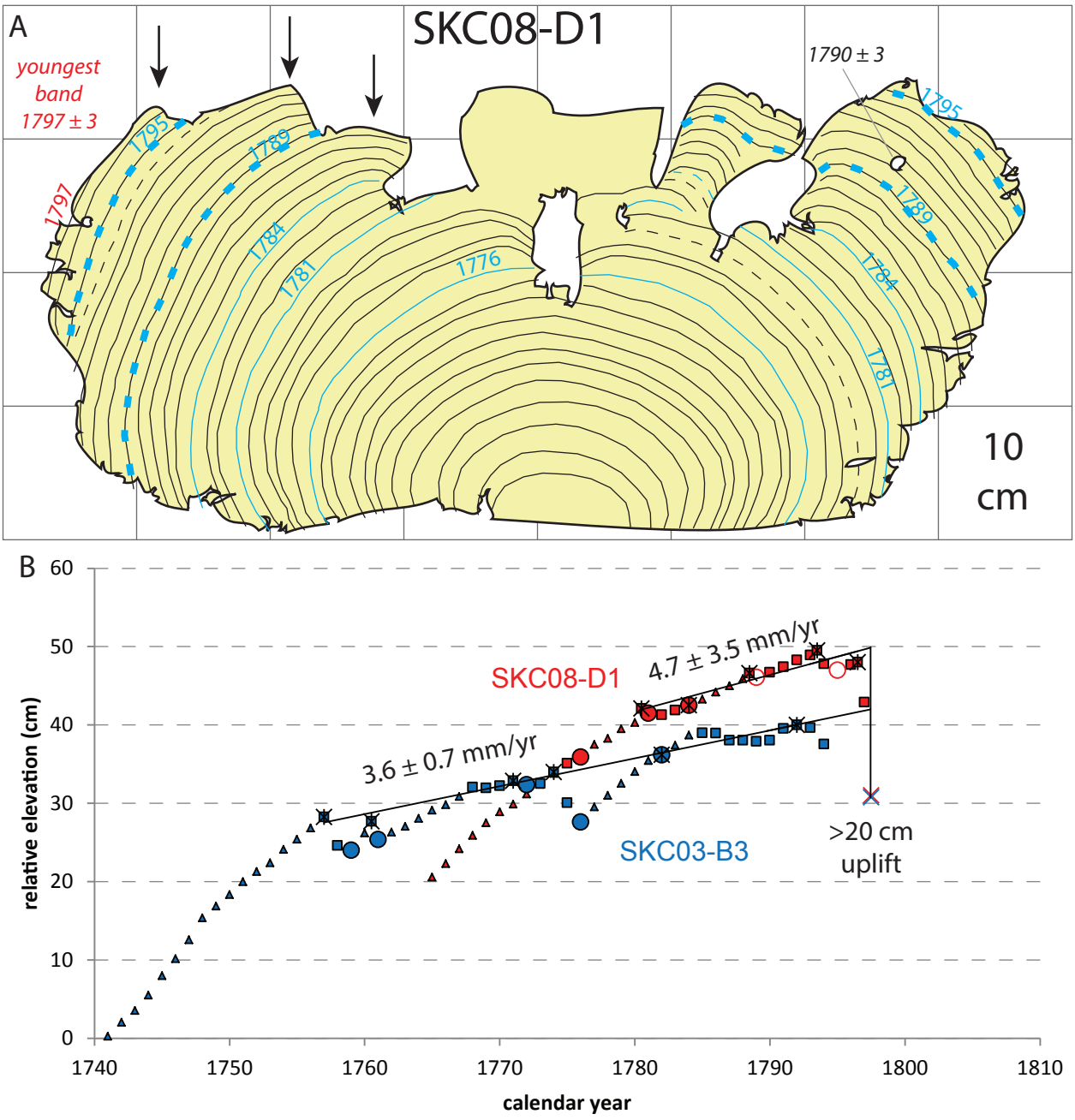

Figure S7. A) Cross section of the Favid microatoll SKC08-D1 from Sikici D. Symbology as in Fig. S5. Large-corallite species tend to yield more precise U-Th dates, and this is no exception: it clearly died due to uplift in the 1797 earthquake. B) Growth history of SKC08-D1 and reinterpreted SKC03-B3. Interseismic subsidence rates are identical within uncertainty, but the longer B3 record provides a more tightly constrained estimate. As is common, the HLS for the Favid D1 was about 10 cm higher than for the *Porites sp.* B3.

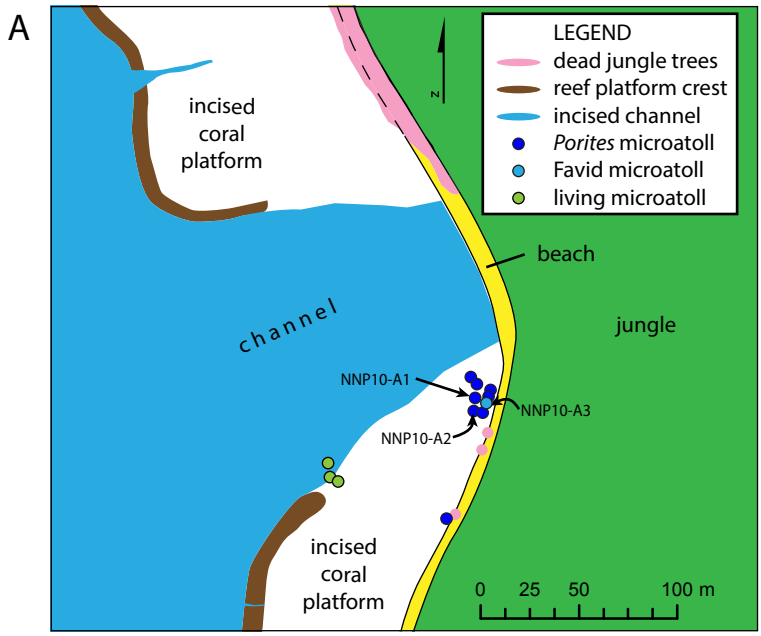

Figure S8. Data from the North North Pagai site.

A) Map of the site on the northwest coast of North Pagai island. The wide channel through the ancient coral platform suggests that there was formerly a freshwater stream outflow in this area. A band of dead trees along the beach is evidence of ongoing interseismic subsidence. There is a single population of fossil microatolls at this site, mostly *Porites sp.* but with a few Favids.

B) Cross sections of slabs NNP10-A1, A2, and A3 (symbology as in Fig. S5A). Dates are consistent with uplift and death of all corals during the 1833 earthquake. A subset of the *Porites* coral population have a high satellite ring around the middle, as illustrated by sample A2. The satellite growth apparently grew contemporaneously with the outer perimeter, though it is considerably higher (inner satellite growths frequently have higher HLS than the coral's outer perimeter, perhaps due to water pooling inside the microatoll). The number of bands in the satellite indicate that about three bands must have been eroded off the perimeter.

C) Growth histories of A1 and A2 (symbology as in Fig. S5B). A2 records a faster subsidence rate than A1, though there is considerable overlap between the confidence intervals. We adopt an average rate of 5.4 mm/yr for this site, which is consistent with both records. One other possible scenario is that the population of corals with morphology similar to A2 (i.e. with inner satellite heads) were uplifted and died in 1797, while the A1 population grew later and died in 1833. This scenario would explain the differing morphologies and subsidence rates and would also be consistent with the U-Th dates. However, due to the strong correspondence in the pattern of oceanographic die-downs on the two heads, contemporaneous growth of A1 and A2 is the more likely scenario. Most importantly, adopting the non-contemporaneous scenario would not significantly alter our final results: a 40-cm 1797 uplift preceded by 6.8 mm/yr of subsidence is consistent with the regional pattern.

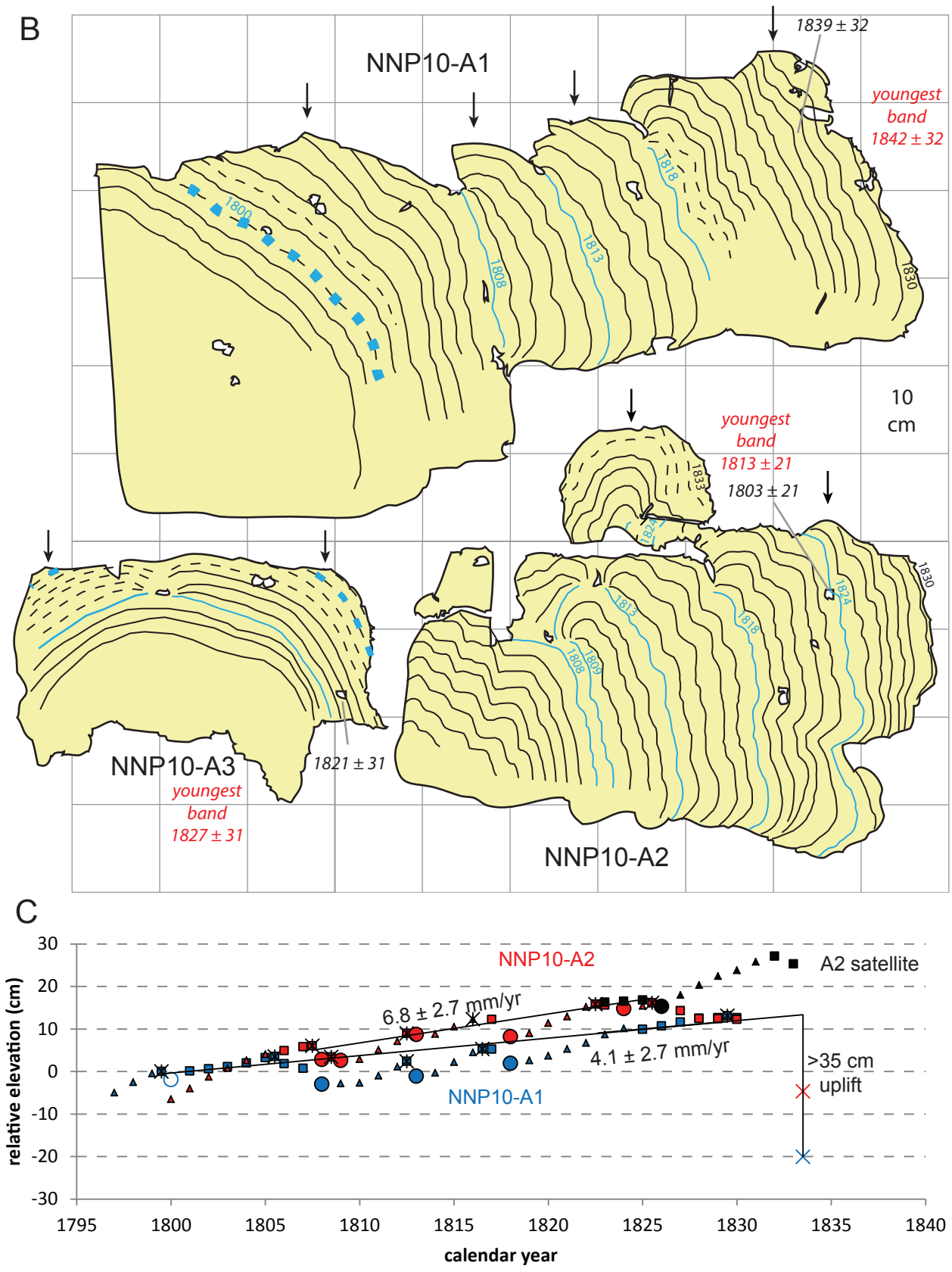

Figure S8 (continued)

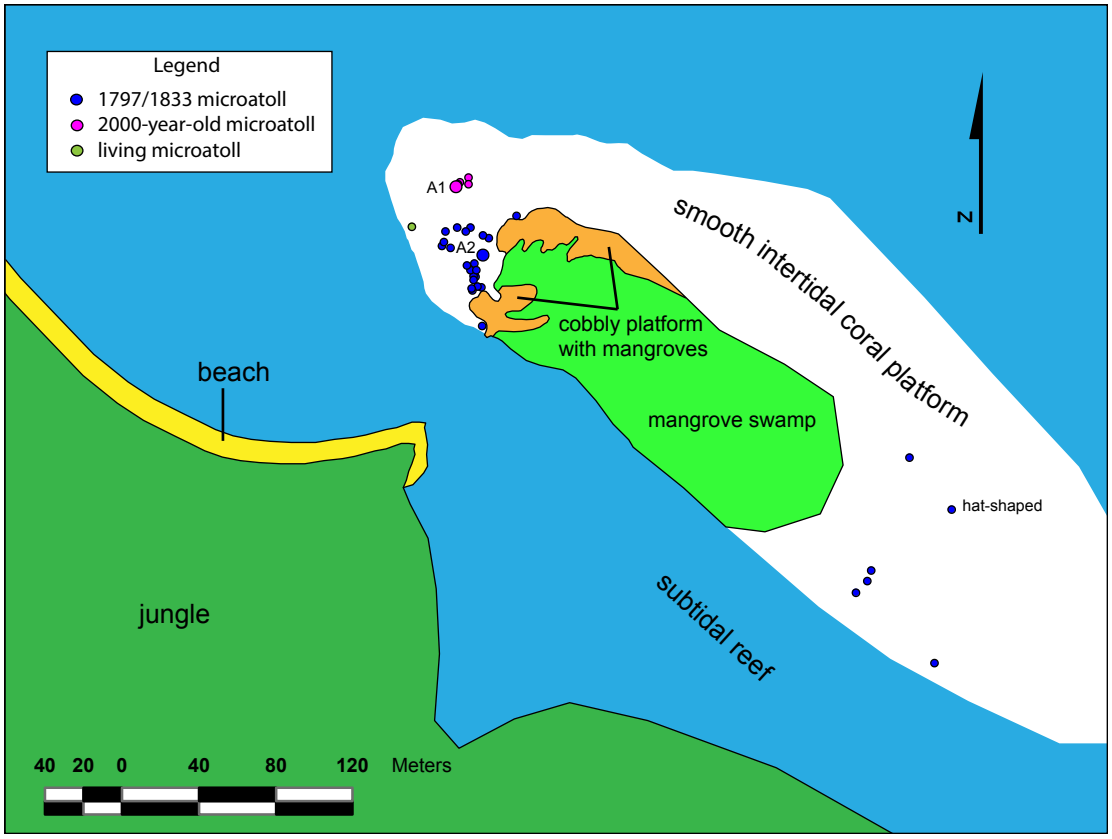

Figure S9. Map of Basua site A on a small islet off the east coast of South Pagai island. The primary population of microatolls was uplifted and died during the 1797 and 1833 earthquakes. Though the sampled specimen A2 was cup-shaped, an un-sampled hat-shaped microatoll of the same generation illustrates that both great earthquakes produced uplift at this site. A lower-elevation population of microatolls is more than 2000 years old (date from BSA03-A1 presented by *Philibosian et al.* [2012]).

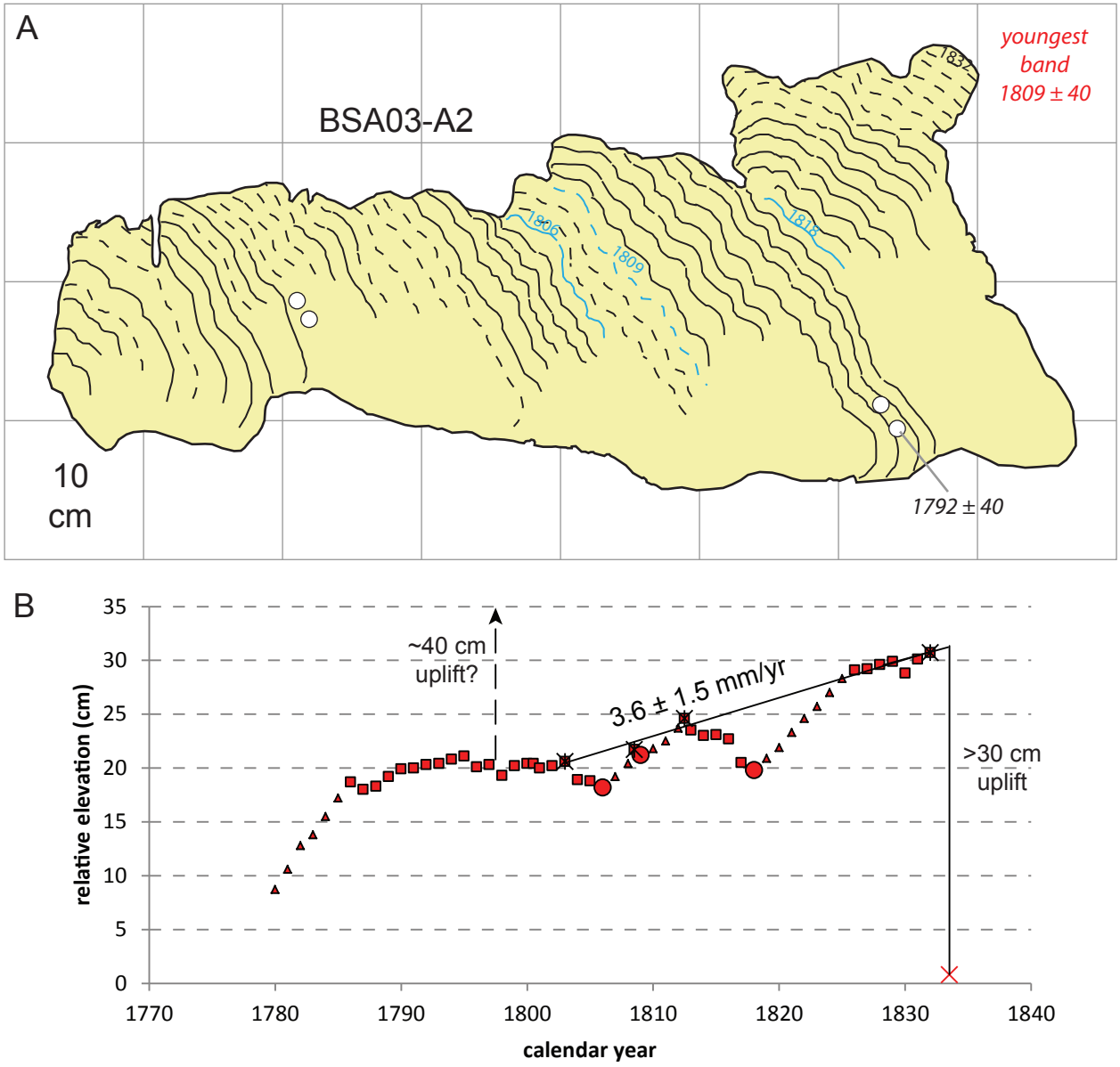

Figure S10. A) Cross section of a microatoll from Basua (symbology as in Fig. S5A). This slab was collected in 2003 but not included in previous papers due to the high uncertainty of its date of death, which encompasses both 1797 and 1833. We infer that this microatoll died in 1833, as this interpretation matches its large die-down with the robust regional 1818 die-down. B) Growth history of BSA03-A2 (symbology as in Fig. S5B). Nearby sites uplifted ~40 cm in 1797, but this coral would not yet have reached HLS before the earthquake, so it recorded a smaller die-down (the inner hemisphere has since been significantly eroded).

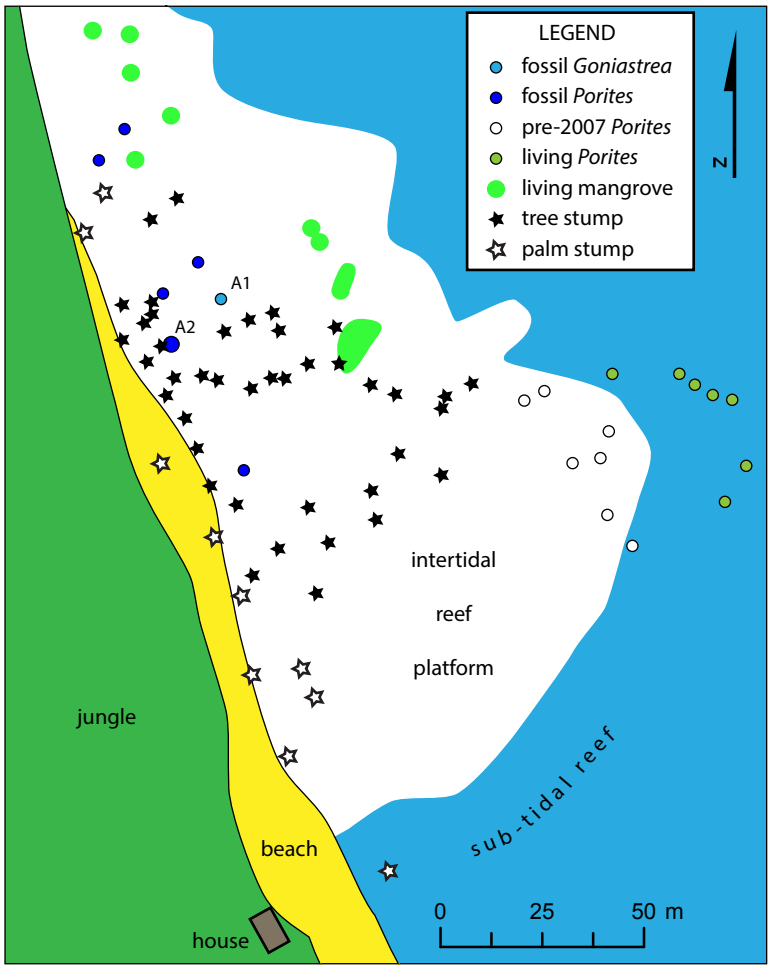

Figure S11. Map of Pecah Belah site A, on the northern coast of the islet Pecah Belah in the South Pagai archipelago. Two sampled microatolls represent a population that died due to uplift in the 1833 earthquake. White circles indicate microatolls which died due to uplift in the 2007 earthquake; green circles indicate those which were growing at lower elevation and survived. A broad swath of jungle trees grew on the reef platform (likely following the 1833 uplift) but have since died due to interseismic submergence. The 68-cm 2007 uplift [*Sieh et al.* 2008] was insufficient to raise the platform above high tide, as would be required to support jungle trees. In contrast, we estimate that the uplift in 1833 was about 1.2 meters.

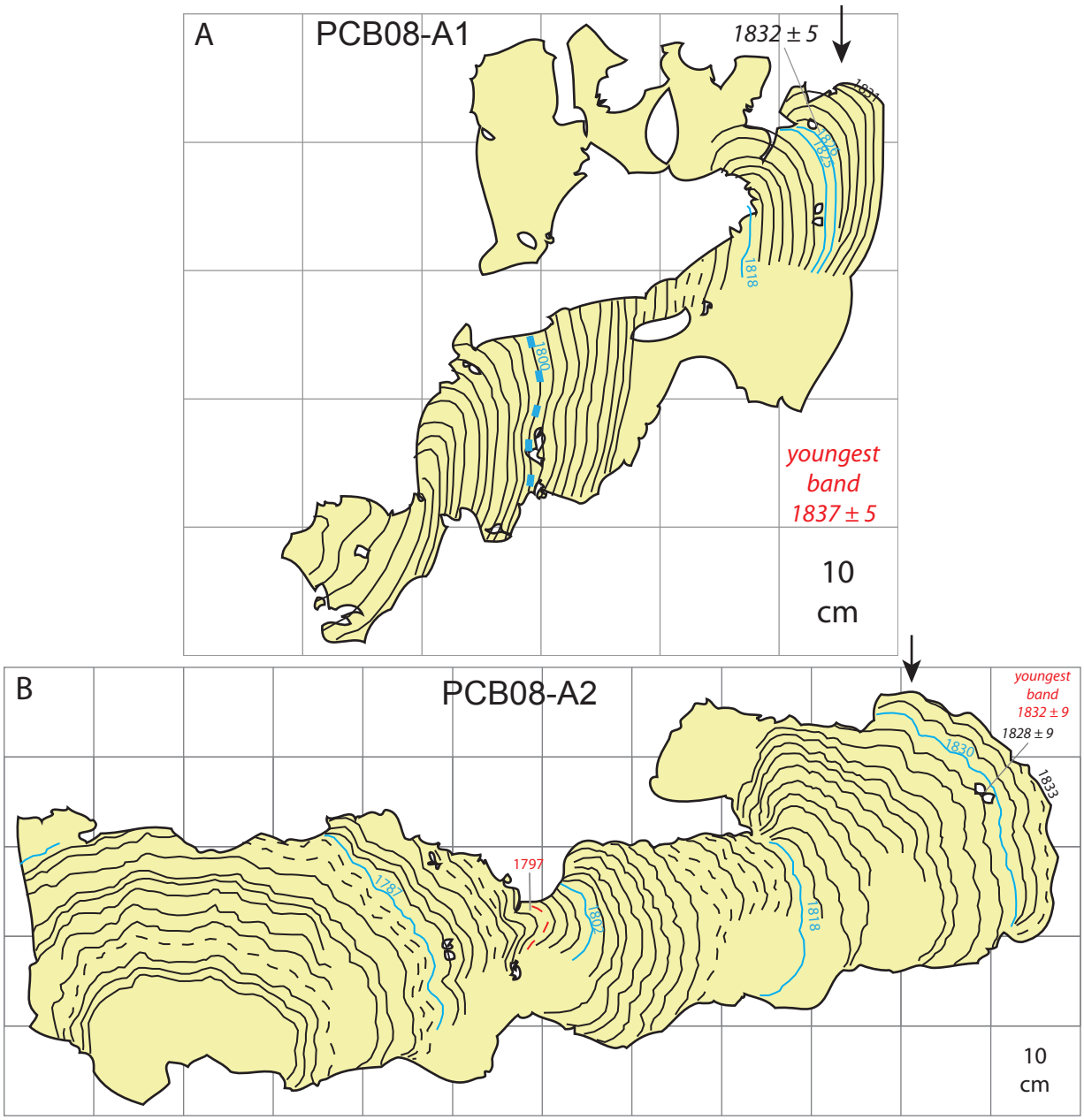

Figure S12. Cross sections and growth histories from Pecah Belah (symbology as in Fig. S5). A) PCB08-A1 is a *Goniastrea sp.* which first hit HLS shortly after the 1797 earthquake, and died due to uplift in the 1833 earthquake. B) PCB08-A2 is a *Porites sp.* which experienced a 15-cm die-down in 1797 and died completely in 1833. C) Cross section of PCB08-B2 from Pecah Belah B, a nearby site that will be presented in a future paper. The surface of this micro-atoll has been significantly eroded, but it suggests a low subsidence rate before it was killed by a large uplift in 1833. D) Comparative growth history of all three PCB coral samples. B2 almost certainly settled ~20 cm into the muddy substrate (other microatolls of this generation were at somewhat higher elevations.) A1 may have settled as well, since *Goniastrea sp.* frequently can survive higher than *Porites sp.* The 20 years of unhindered upward growth of B2 after it first hit HLS in 1774 suggests that the interseismic subsidence rate before 1797 was relatively high, but this is an uncertain result.

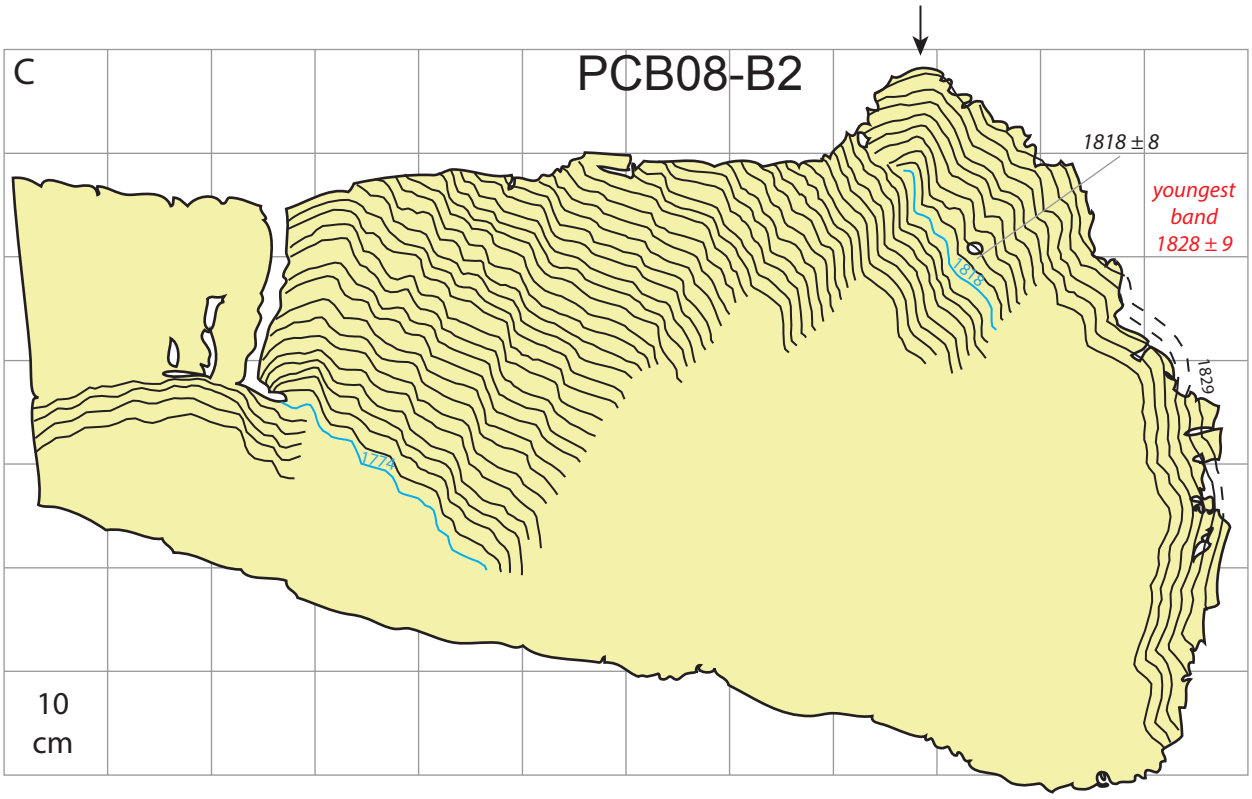

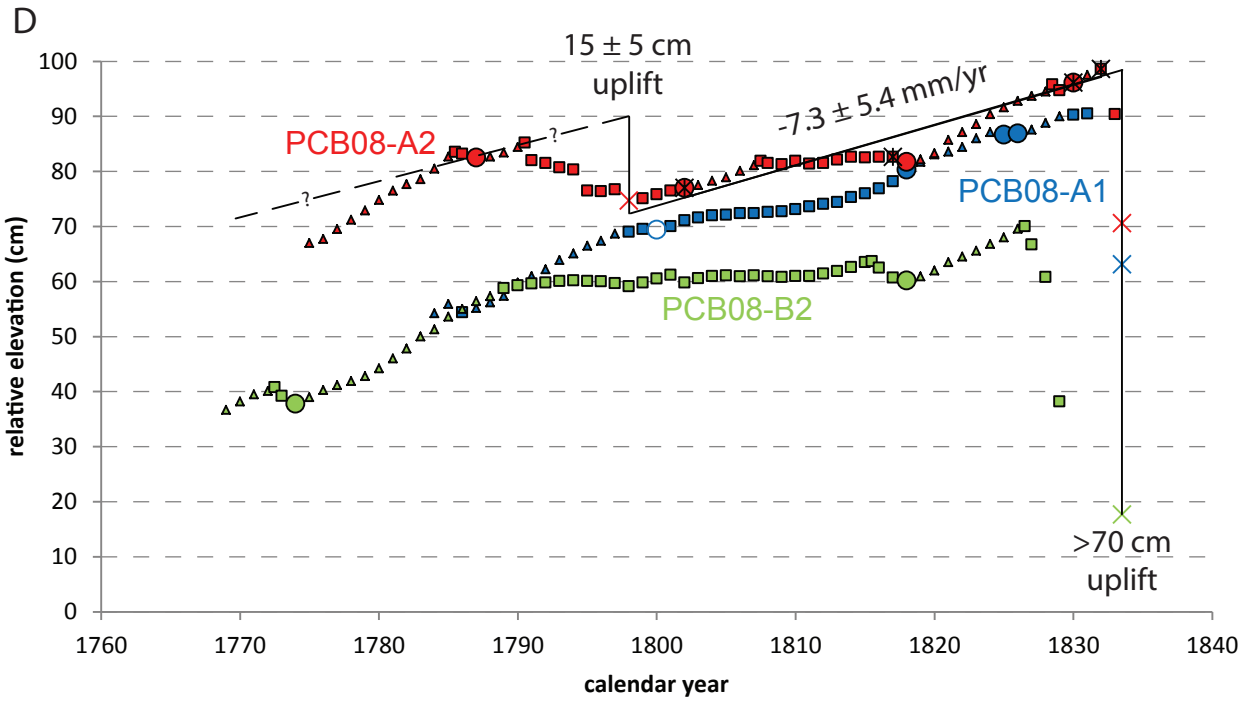

Figure S12 (continued)

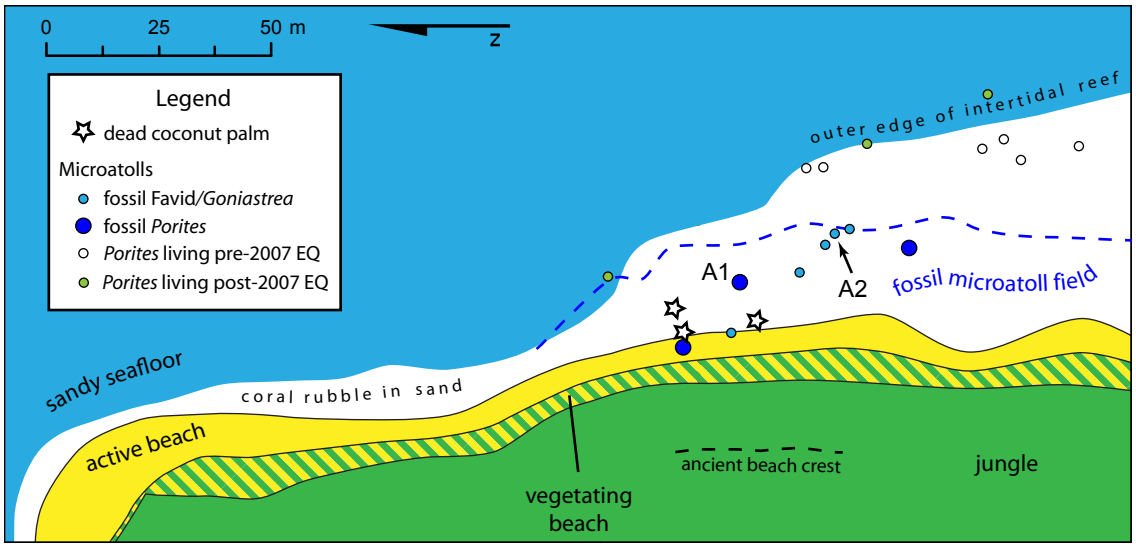

Figure S13. Data from Pulau Simaturugogo, an islet in the South Pagai archipelago.

A) Map of the site on the west side of the islet. During the 2007 earthquake the site was uplifted 45 cm, killing many living corals. Between that time and our visit in 2008, the old beach began to vegetate and a new beach formed at a lower elevation. We sampled two micro-atolls from a population near the beach which died due to uplift in the 1797 earthquake. An ancient beach crest (now covered by jungle) probably corresponds to the fossil coral population.

B) Cross sections of *Porites* A1 and *Goniastrea* A2 from Simaturugogo (symbology as in Fig. S5A). The innermost part of A1 appears to be tilted, so we do not include the growth history before 1742 in our analysis (the head tilted and possibly rolled into deeper water in about 1742).

C) Growth histories of the two microatolls (symbology as in Fig. S5B). The very low average subsidence rate of A1 after 1757 seems inconsistent with the preceding much faster subsidence (1747–1757) and the moderate subsidence rate recorded by A2 (1776–1797). We infer that the HLS of A1 was controlled by a very local pool above the open ocean HLS between 1747 and 1776. By excluding the fit points within that period (orange stars) and including the fit point before 1747 (pink star), we obtain a subsidence rate for A1 which is consistent with A2. We use the rate derived from A2 as the pre-1797 rate for this site, since the interpretation of A1 is questionable.

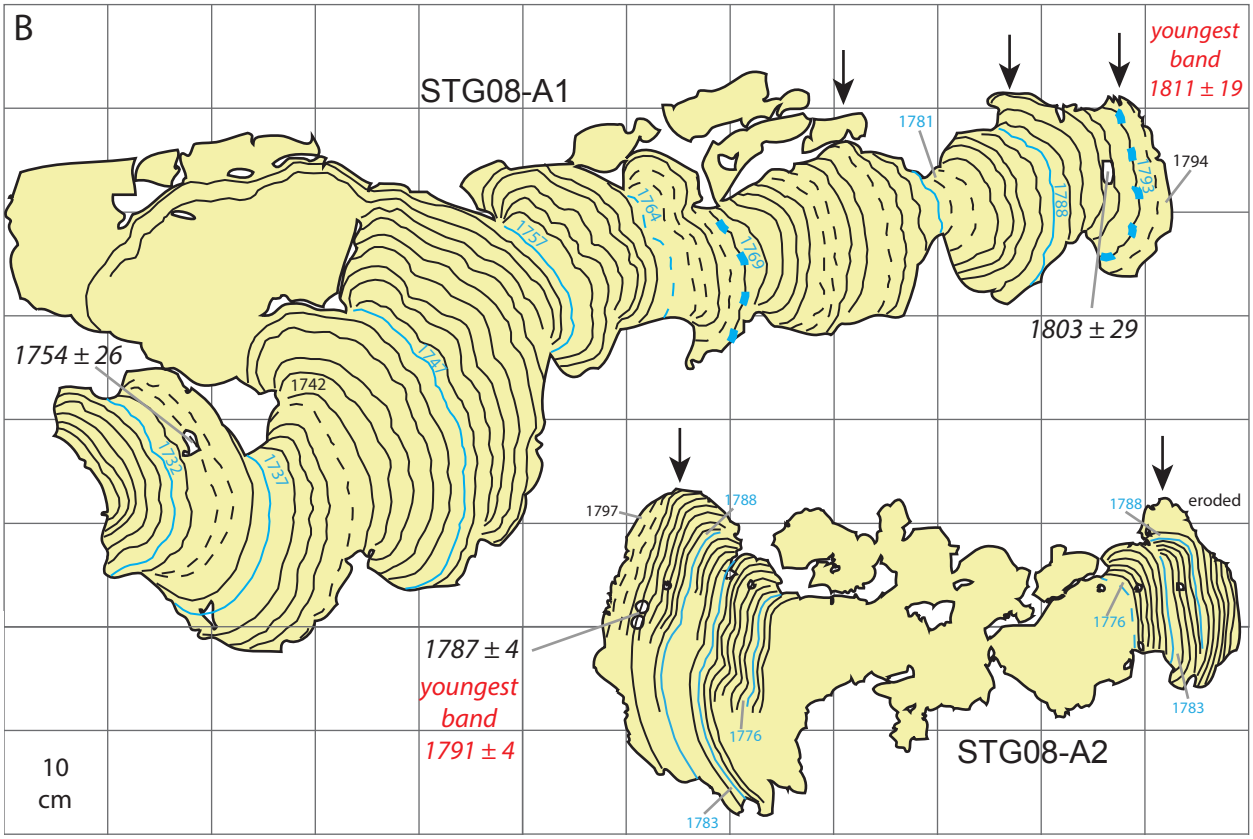

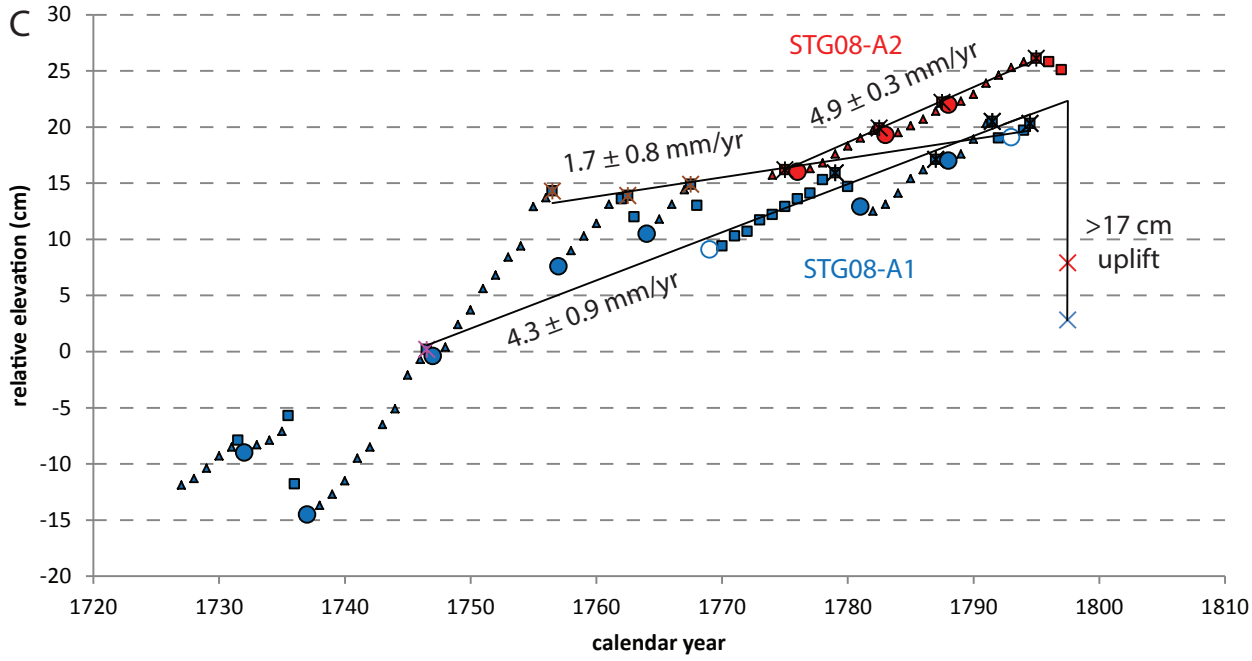

Figure S13 (continued)

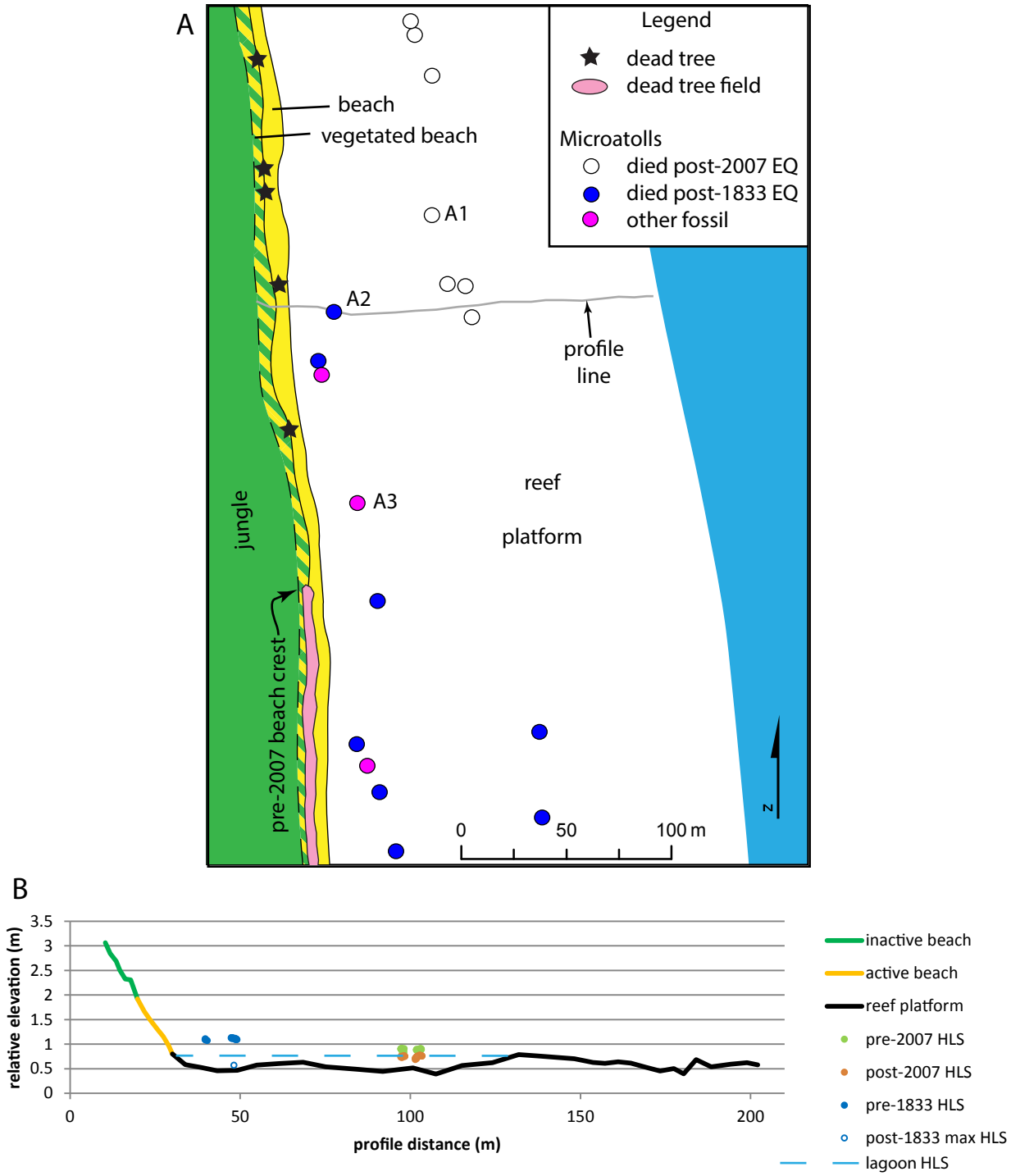

Figure S14. A) Map of the Simungguk site, on the east side of the southernmost islet in the South Pagai archipelago. B) Elevation profile illustrating that corals survived in a lagoon pool after the 2007 uplift. The corals since died for other reasons (likely bleaching due to the hot, shallow lagoon environment). The abandoned beach crest about 1 meter higher than the active crest implies that the 2007 uplift was significantly larger than the 15-cm die-down on the modern corals suggests. The base of coral head A2 could have similarly survived in the lagoon pool for a short time after the 1833 uplift (uncertain due to erosion of the coral surface.)

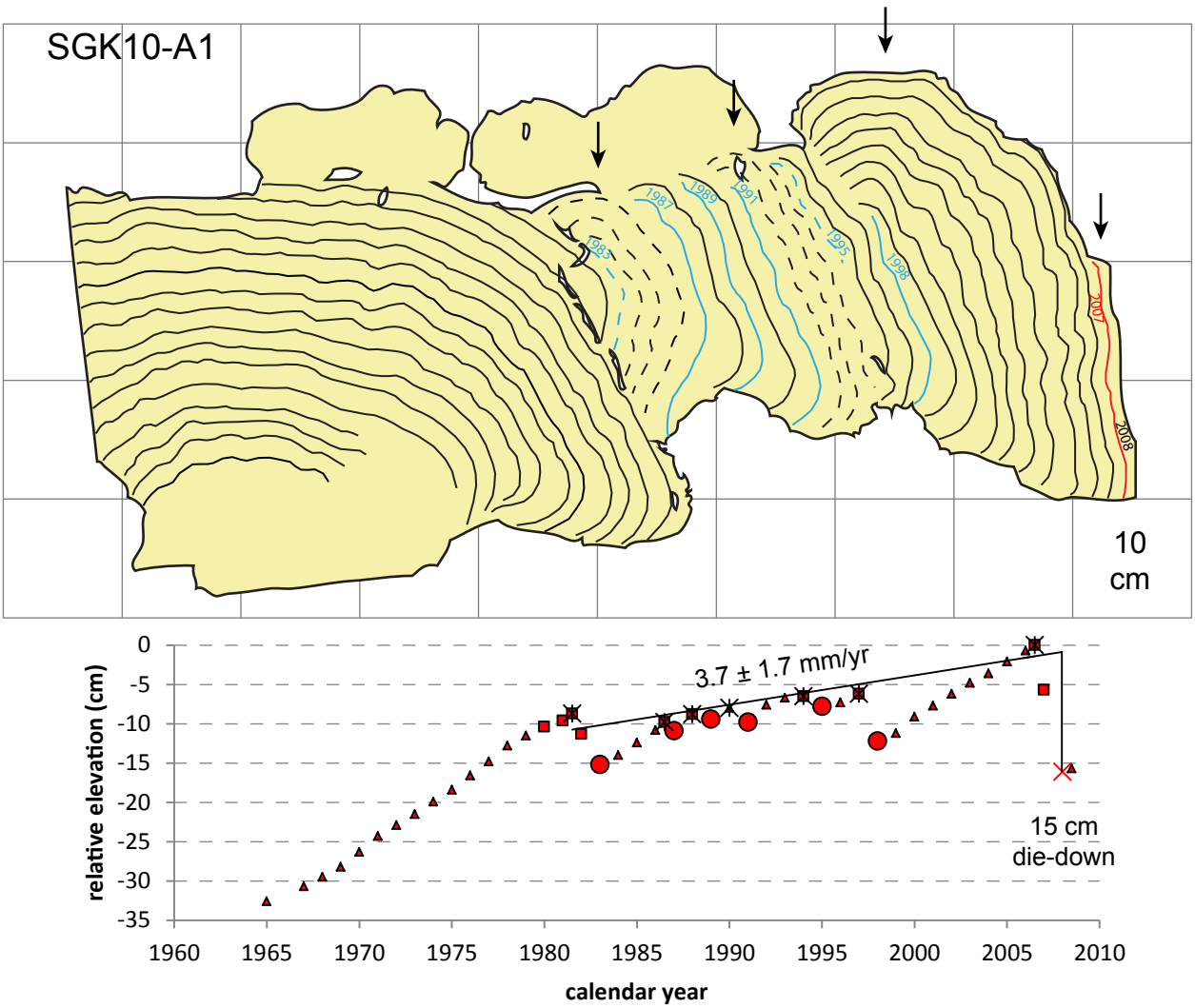

Figure S15. Cross section and growth history of modern slab SGK10-A1 from Simungguk (symbology as in Fig. S5). After 25 years of moderate interseismic subsidence, the 2007 earthquake caused a 15-cm die-down. Though the actual uplift was likely greater than the height of the living coral perimeter, the lagoon pool held water substantially higher than the ocean level and permitted the lower 20 cm of coral surface to continue growing. After about 1 year of post-earthquake growth, this coral died completely.

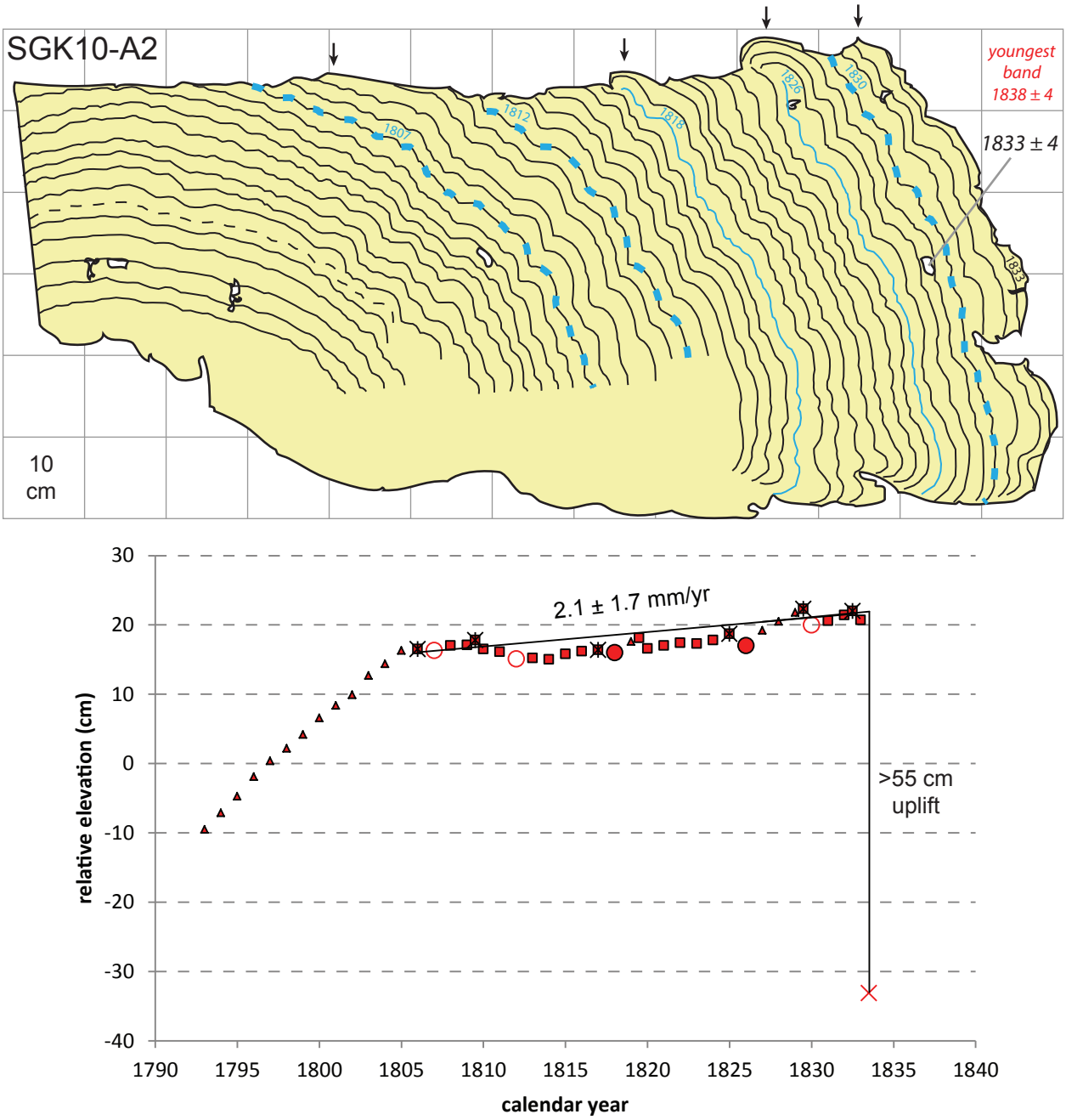

Figure S16. Cross section and growth history of "fossil" slab SGK10-A2 from Simungguk (symbology as in Fig. S5). The subsidence rate leading up to the uplift and death in 1833 appears to have been lower than the rate before the 2007 earthquake. The lowest 15–20 cm of the outer perimeter is below the lagoon-controlled HLS and could have survived after 1833, though there is no positive evidence that it did.

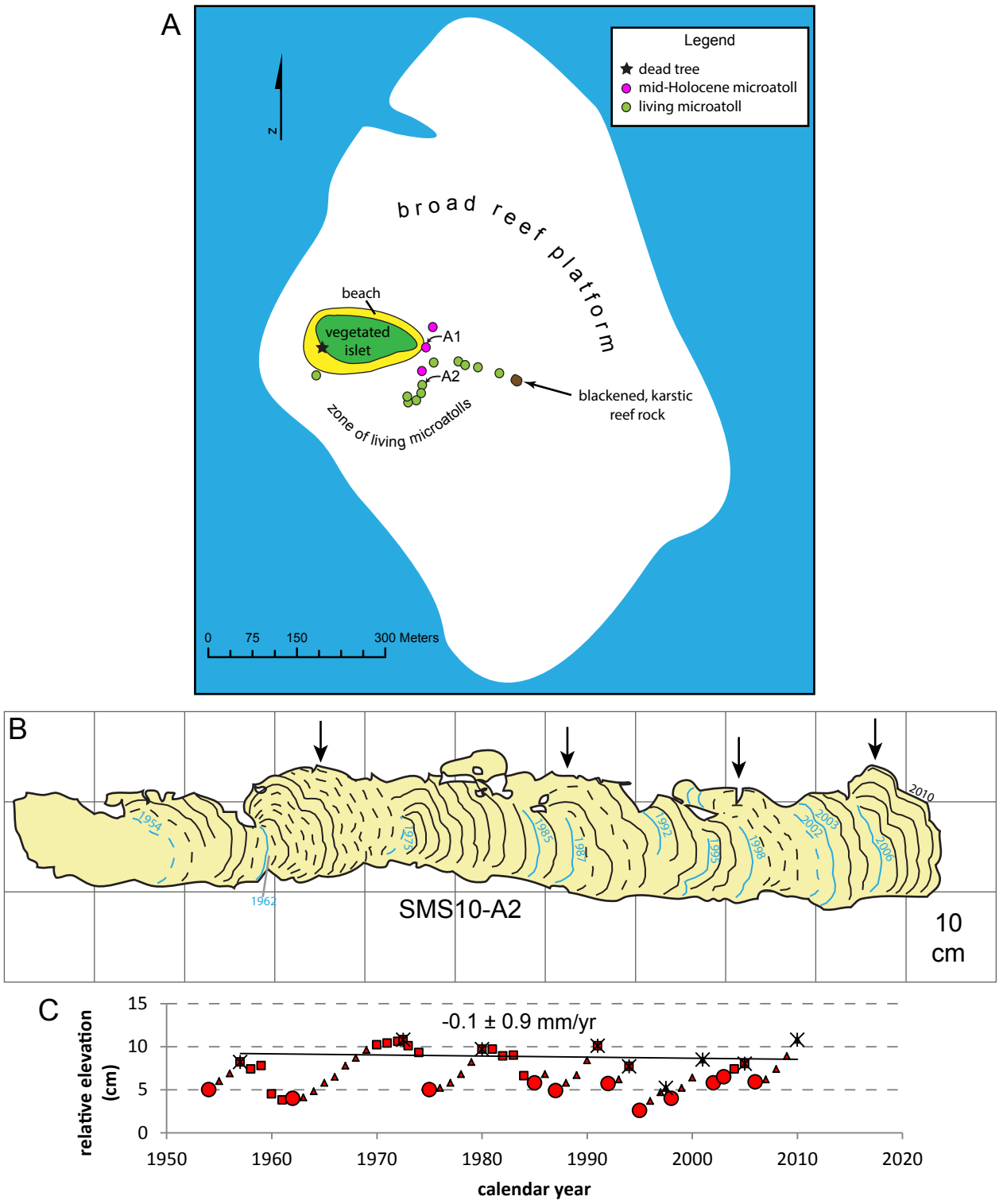

Figure S17. Data from Pulau Simasin, a small islet off the north coast of Siberut. A) Map of the site. Much of the broad reef platform is covered with living microatolls. A small group of "fossil" microatolls dates to the mid-Holocene (date from SMS10-A1 presented by *Philibosian et al.* [2012]). B) Cross section and C) growth history of modern microatoll SMS10-A2, showing essentially stable relative sea level for the past 55 years (symbology as in Fig. S5).

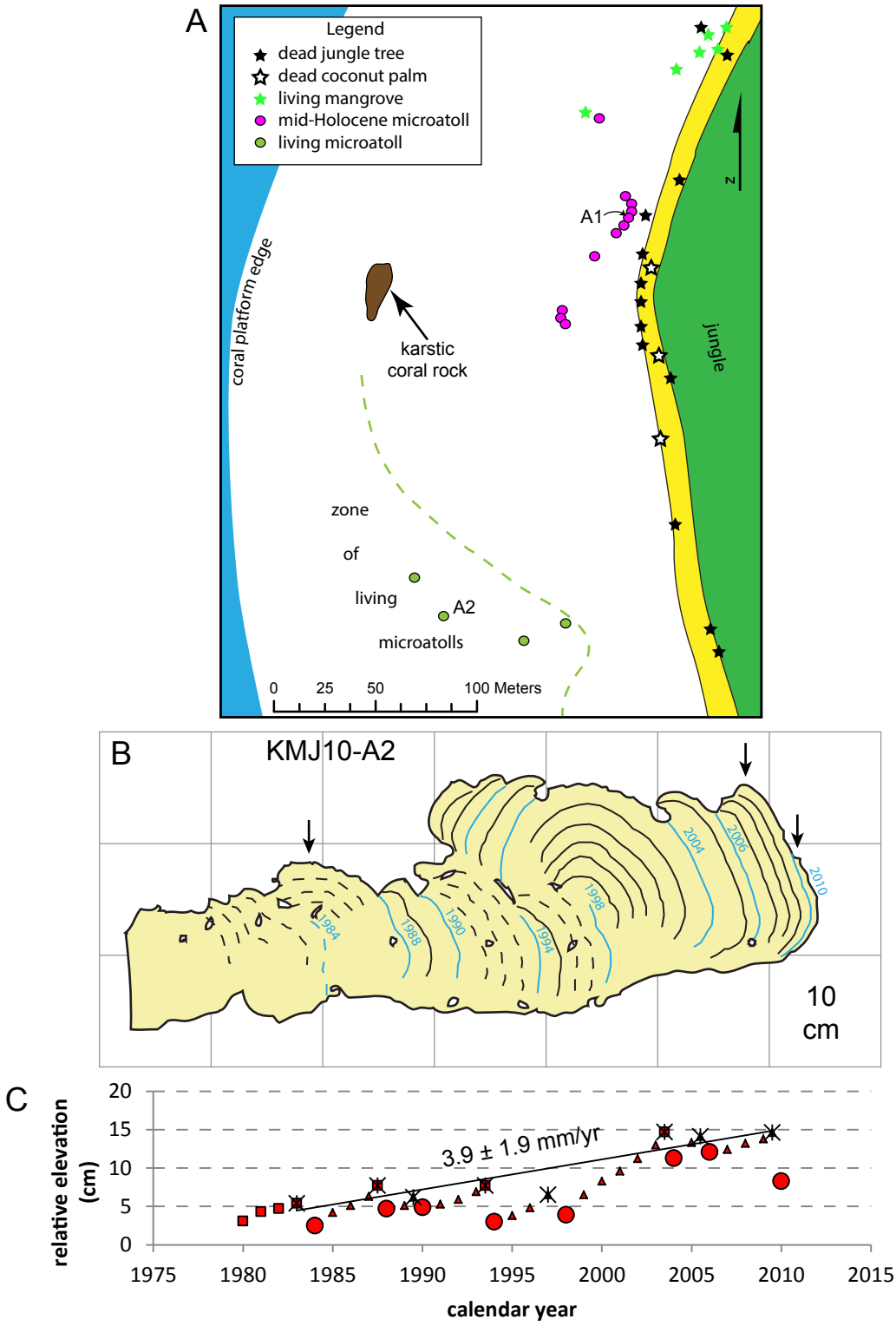

Figure S18. Data from Pulau Karangmadjat, a small island in the archipelago south of Siberut. A) Map of the site on the northwest side of Pulau Karangmadjat. A population of "fossil" microatolls dates to the mid-Holocene (date from KMJ10-A1 presented by *Philibosian et al.* [2012]). B) Cross section and C) growth history of the living microatoll KMJ10-A2, which records a moderate rate of interseismic subsidence. Symbology as in Fig. S5.

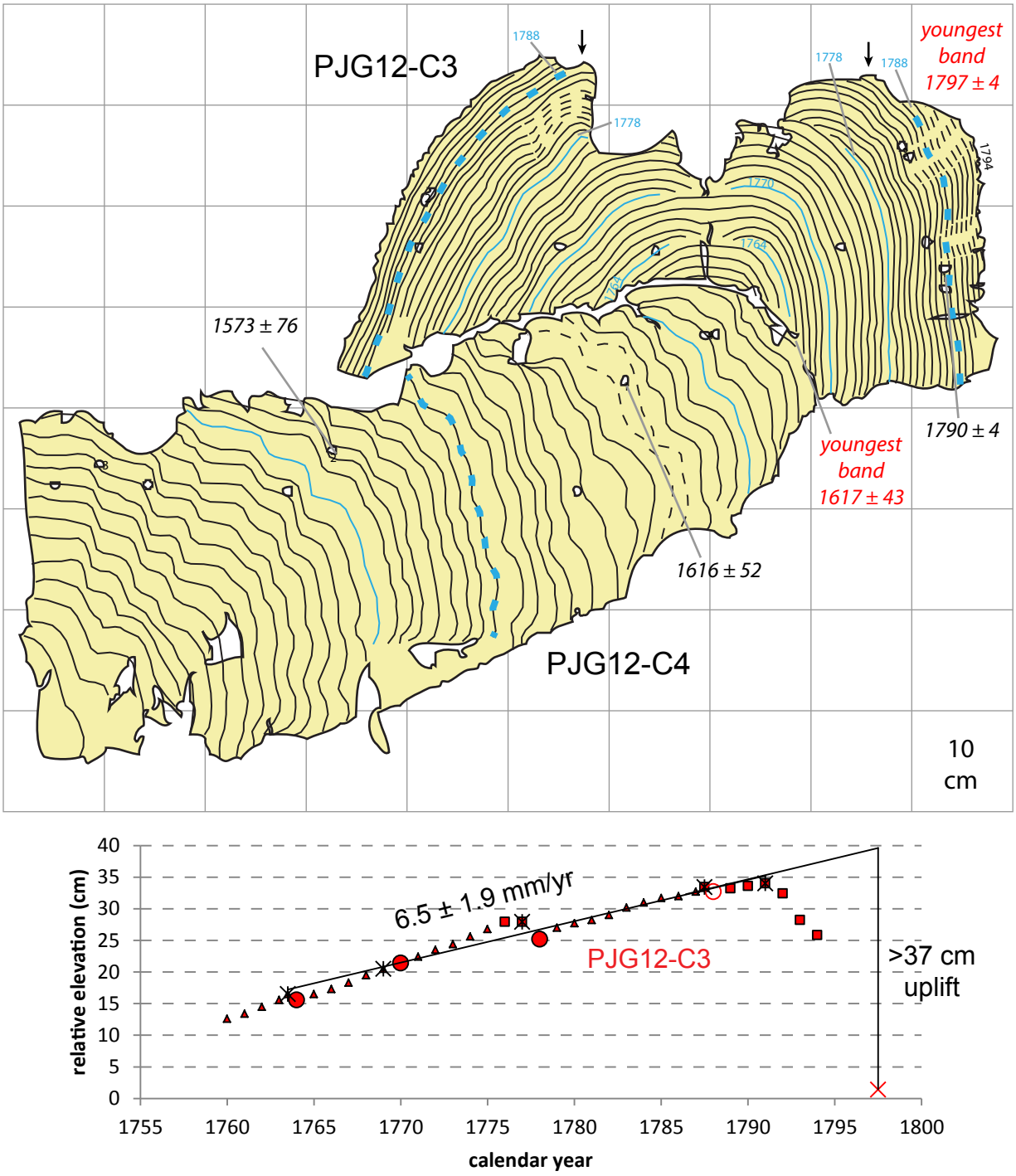

Figure S19. "Fossil" microatolls from Pulau Panjang, an island north of Sipora (symbology as in Fig. S5). A) At site PJG-C, a large population of "fossil" Favid microatolls sits at a higher elevation than a population of *Porites* microatolls. This cross section shows a Favid of the higher population (C3) which actually grew on the rim of a *Porites* of the lower population (C4). C4 died in the 17th century (uplifted during an earlier megathrust rupture sequence), and C3 began growing about 1760 after interseismic subsidence had lowered the dead C4 below HLS once more. C3 was uplifted and died during the 1797 earthquake. B) Growth history of C3.

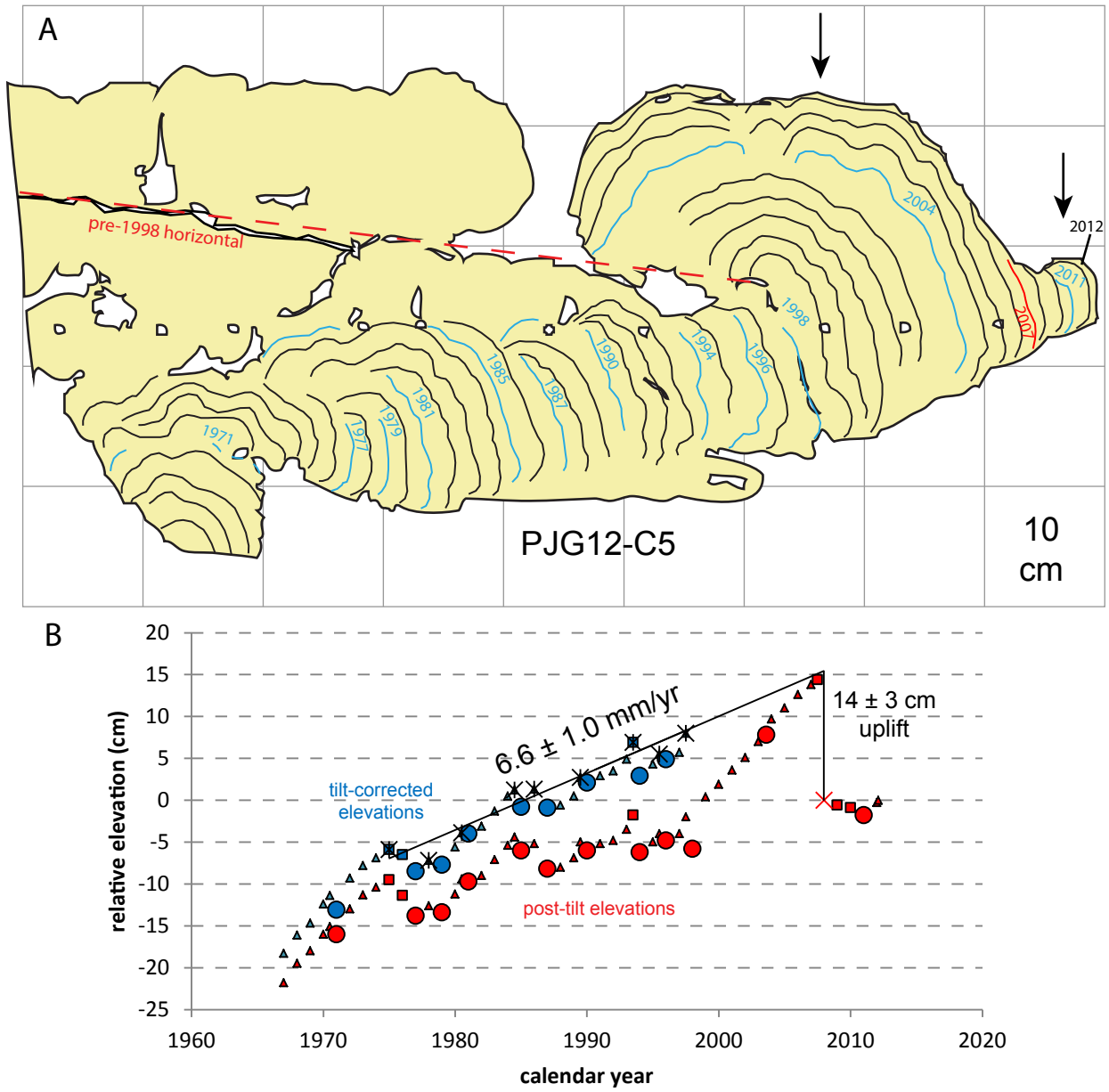

Figure S20. Modern coral data from Pulau Panjang (symbology as in Fig. S5). A) Cross section of the living microatoll PJG12-C5. About 14 cm of uplift occurred during the 2007 M_w 7.9 earthquake, which uplifted an area on northern Sipora disconnected from the more extensive uplift on South Pagai during the M_w 8.4 earthquake 12 hours earlier [*Konca et al.* 2008]. The PPNJ cGPS station less than 2 km south recorded 23 cm uplift, suggesting that the uplift dropped off extremely steeply. This and several other modern microatolls at the site record about 2 cm of postseismic uplift since 2007, which is consistent with the PPNJ record (P. Banerjee, pers. comm.) As indicated by a preserved formerly horizontal surface, this microatoll clearly tilted sometime after 1998, lowering this side so that growth did not catch up to HLS again until 2004. B) Growth history of PJG12-C5. Correcting the pre-1998 record for the tilt yields an accurate interseismic subsidence rate. As the annual bands are far clearer and the tracking of HLS is more certain on this sample than on Pj03-A1 [*Natawidjaja et al.* 2007], we use this record alone to calculate the modern interseismic subsidence rate on Pulau Panjang.

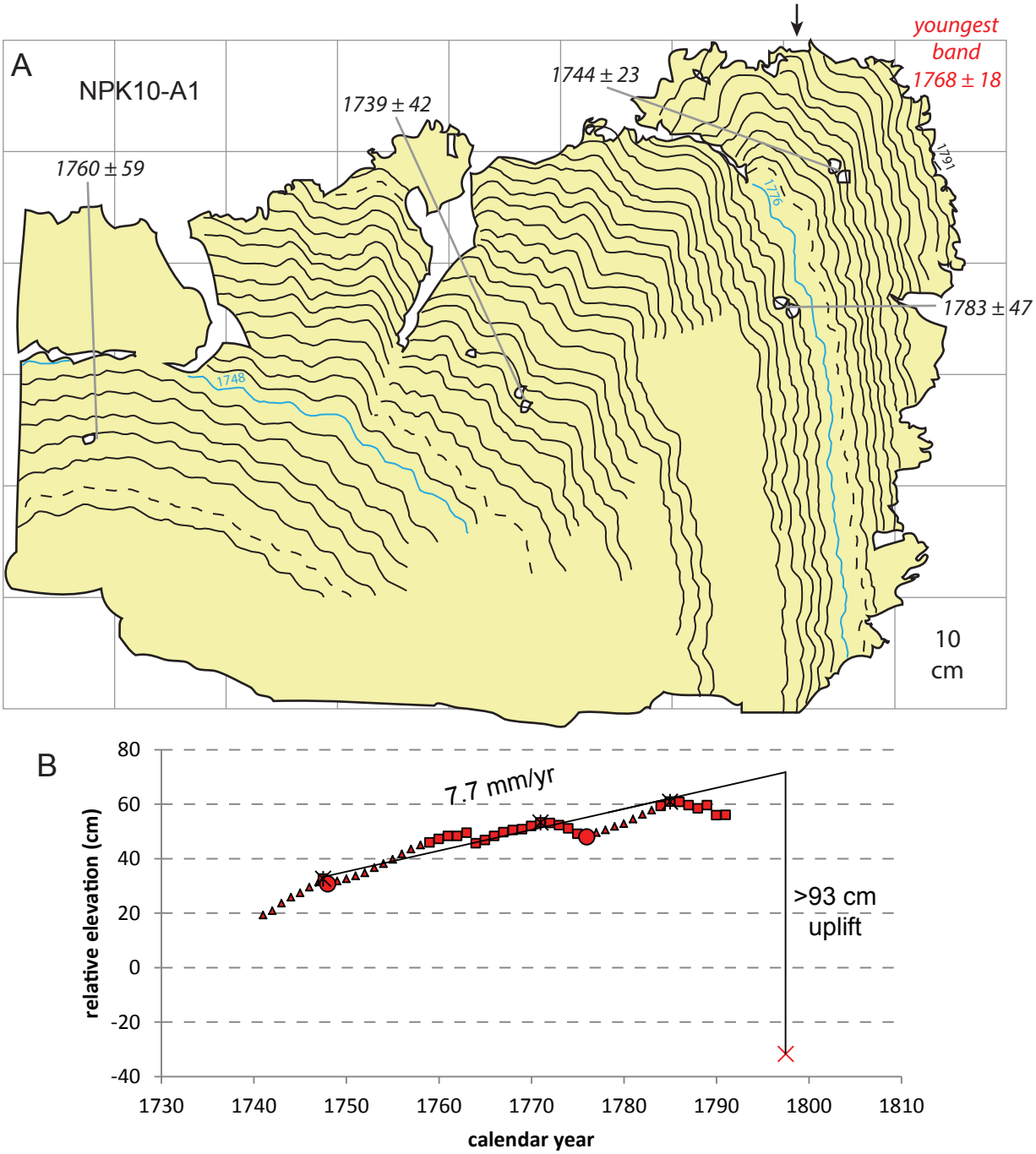

Figure S21. Data from North Pukarayat, on the south coast of Sipora (symbology as in Fig. S5). A) Cross section of a large microatoll which was part of a population with similar morphology. A weighted average of four U-Th dates suggests that the head died in the mid-1700s. Our coral dataset does not support the occurrence of a large tectonic uplift in that period (at many sites, the possibility is specifically excluded.) We infer that this population of corals probably died due to uplift in 1797 (which is inconsistent with only one of the four U-Th dates). Matching the large die-down preserved in this record with the robust regional 1776 die-down requires 6 bands to be eroded from the outer surface. B) Growth history of NPK10-A1. Regardless of precisely when the coral died, it records a high interseismic subsidence rate during the 1700s.

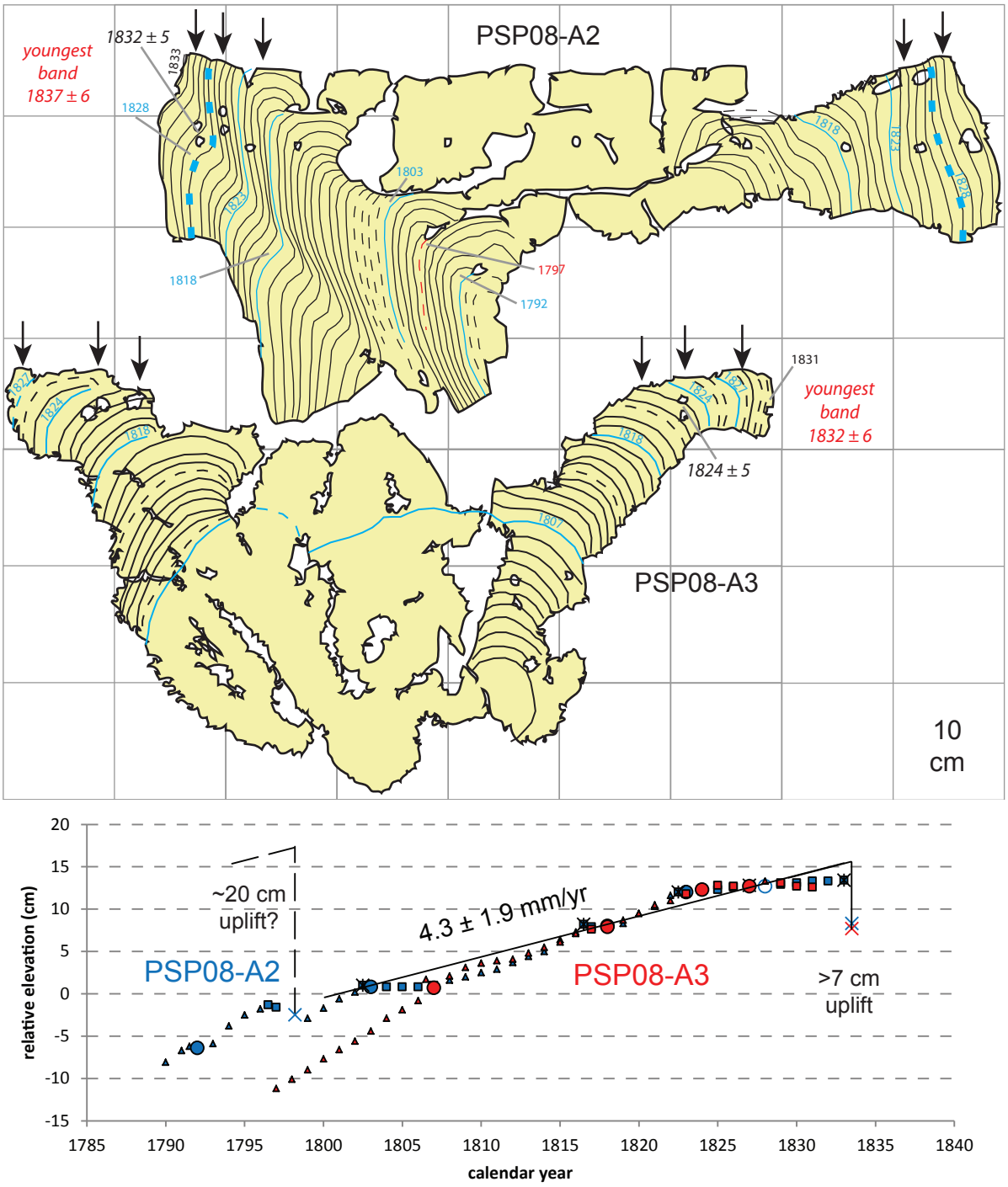

Figure 22. Data from Pasapuat on the north coast of North Pagai (symbology as in Fig. S5). A) Cross sections of *Goniastrea* (A2) and Favid (A3) microatolls which clearly died due to uplift in 1833. A2 also had a small die-down at the time of the 1797 earthquake. However, since other sites in the region suggest that uplift in 1797 was tens of centimeters in this area, we infer that A2 had not actually hit HLS before the 1797 earthquake. The 1792 die-down is so minor that it is quite plausible that it represents a growth irregularity rather than a sea-level-controlled die-down. B) Growth histories of the two microatolls are highly consistent. We derive the interseismic rate from A2 since its record is slightly longer, but we exclude the points before 1797.

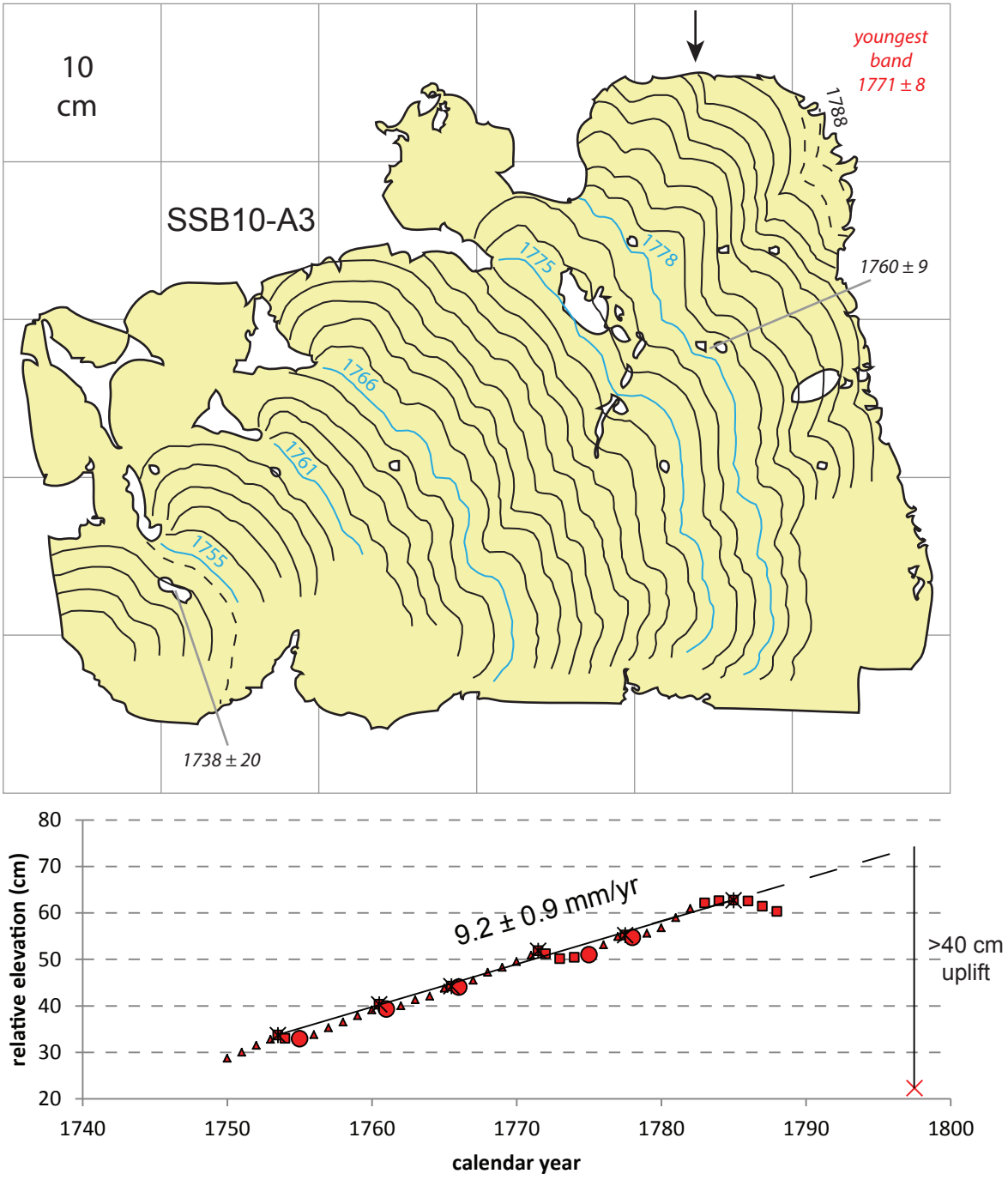

Figure S23. Cross section and growth history of a microatoll from the south coast of Silabusa-beu, a small island west of Silabu Village on North Pagai. Symbology as in Fig. S5. The U-Th ages suggest death in ~1770, but the large population that this specimen came from indicates death due to tectonic uplift, most likely in 1797. Assuming the age uncertainty is underestimated, die-down matching suggests that the youngest preserved band grew in 1788. This interpretation requires that 9 annual bands have been eroded from the outer perimeter of this microatoll, a large but not impossible number. The high pre-1797 interseismic subsidence rate is well-constrained and very similar to the contemporaneous rate at the nearby Silabu site.

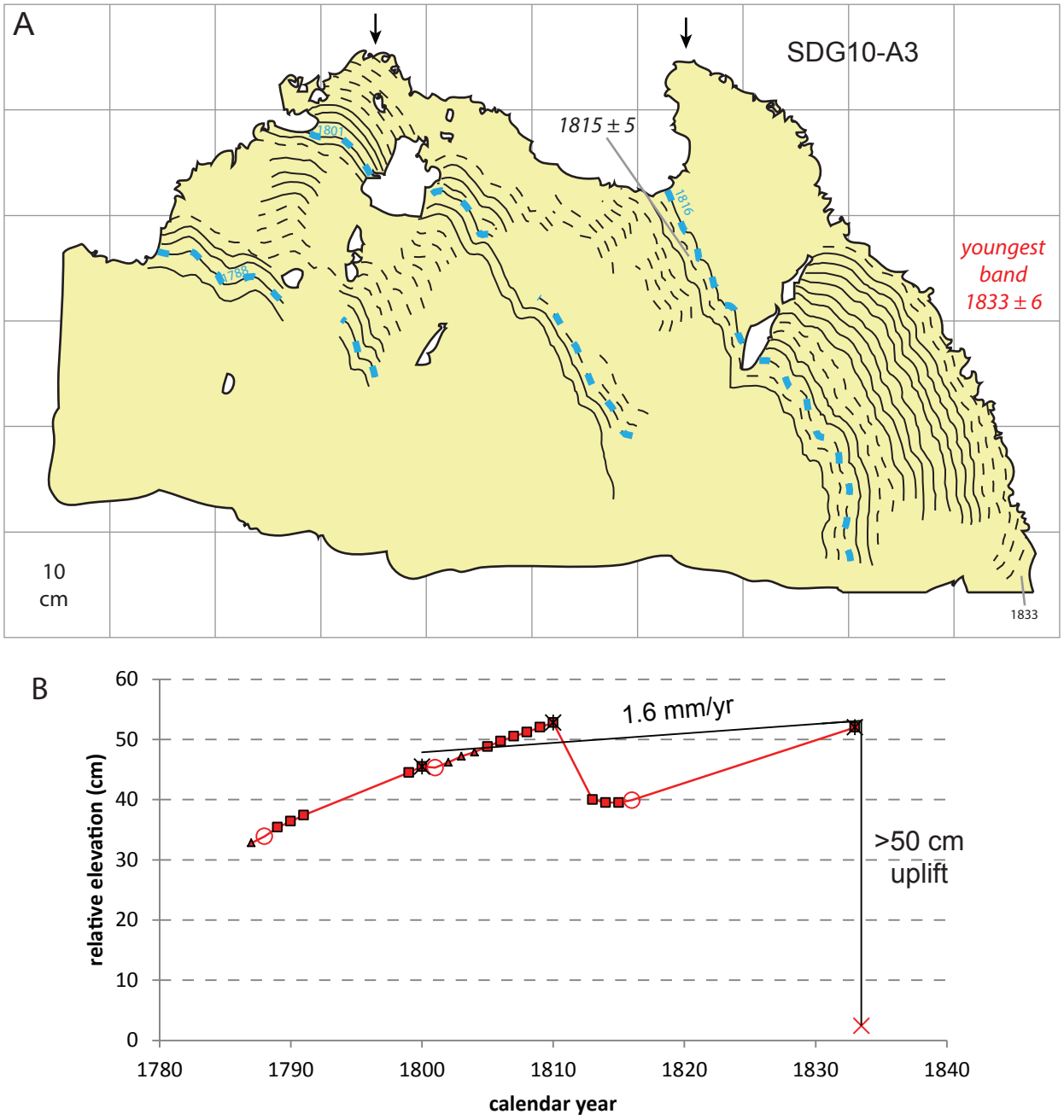

Figure S24. Data from a site on the south side of Sanding Island (symbology as in Fig. S5). A) Cross section of a microatoll with a precise date demonstrating the final uplift and death was in 1833. However, the annual bands are extremely unclear and are largely inferred based on an average growth rate. B) Growth history of SDG10-A3 suggests a low rate of interseismic subsidence. It is clear that there was no significant uplift in 1797. The unimpeded upward growth between the 1788 and 1801 die-downs suggests that the subsidence rate may have been higher before the 1797 earthquake, but this is an uncertain result.

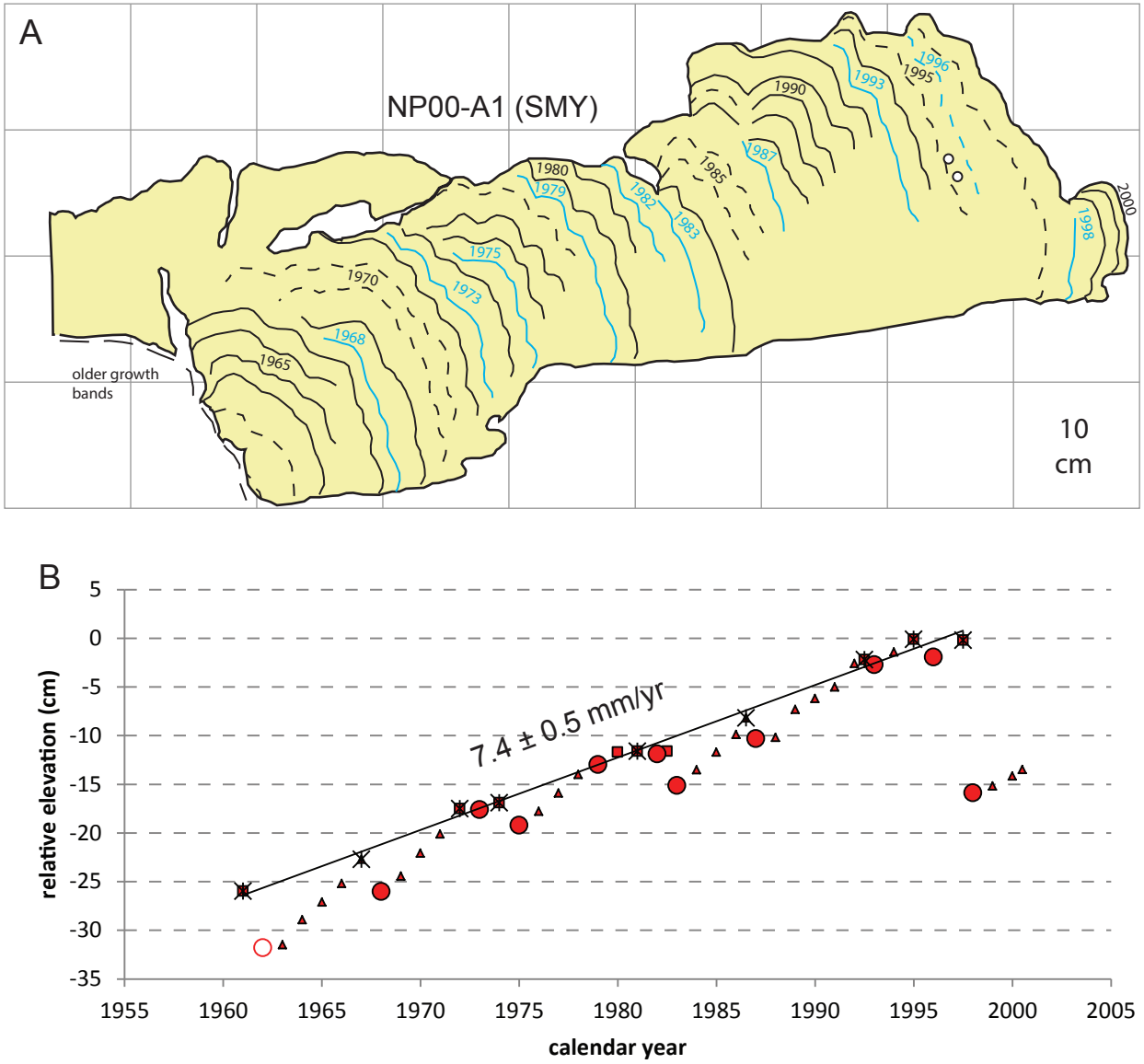

Figure S25. Cross section and growth history of modern coral NP00-A1 from Simanganya (all symbology as in Fig. S5). The growth history reflects a well-constrained moderately high rate of interseismic subsidence during the latter half of the 20th century. When this coral was sampled in 2000, growth had only just begun to recover after the huge 1998 oceanographic die-down. The cross section of this coral was intended to be included by *Sieh et al.* [2008], but omitted due to an oversight. We include it here for completeness.

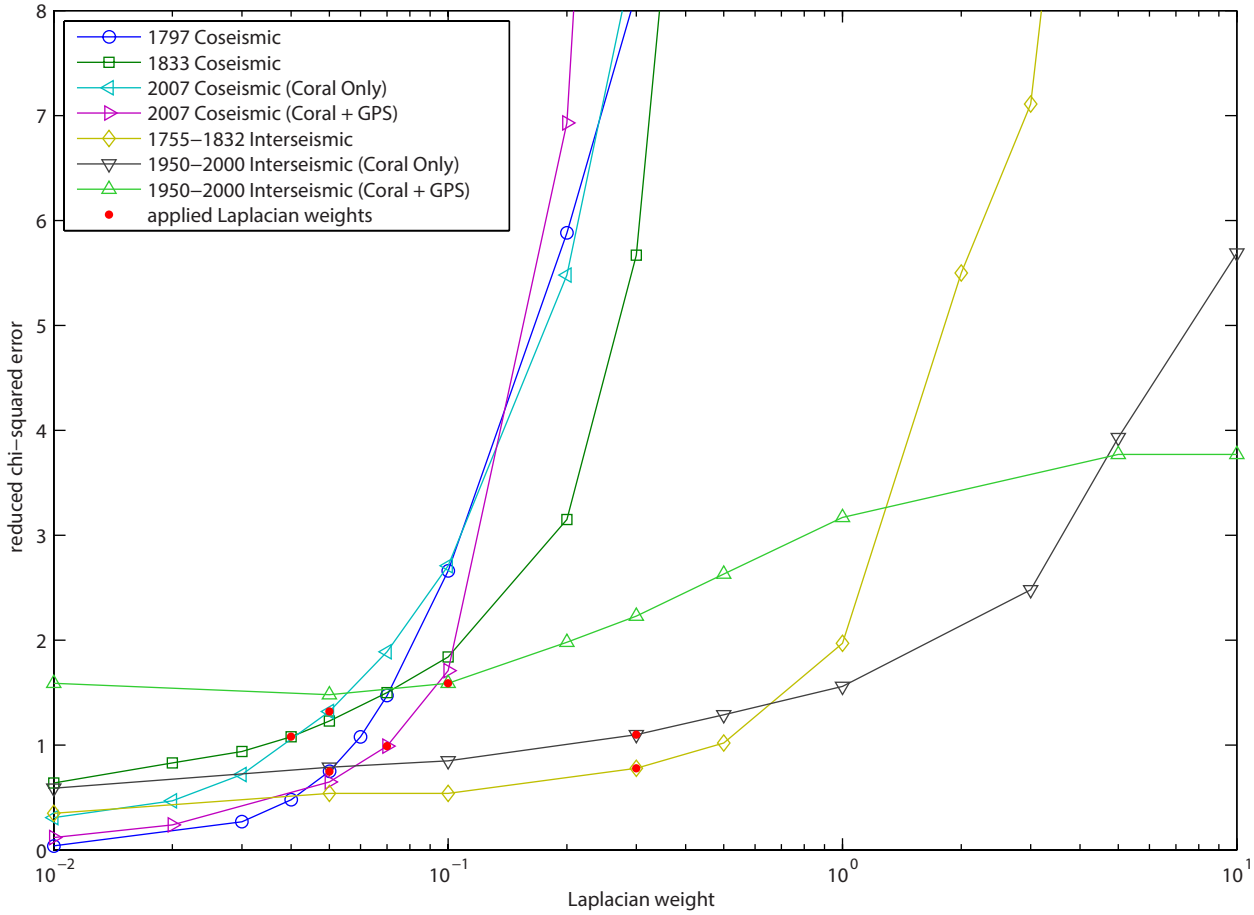

Figure S26. Reduced chi-squared error as a function of the strength of spatial smoothing (overall weight of the Laplacian regularization term). For our final models we applied the weights marked by red dots, which correspond to the strongest smoothing that produces a good fit to the data. These points are generally found near the point of maximum curvature of each curve, in the vicinity of chi-squared values of 1.

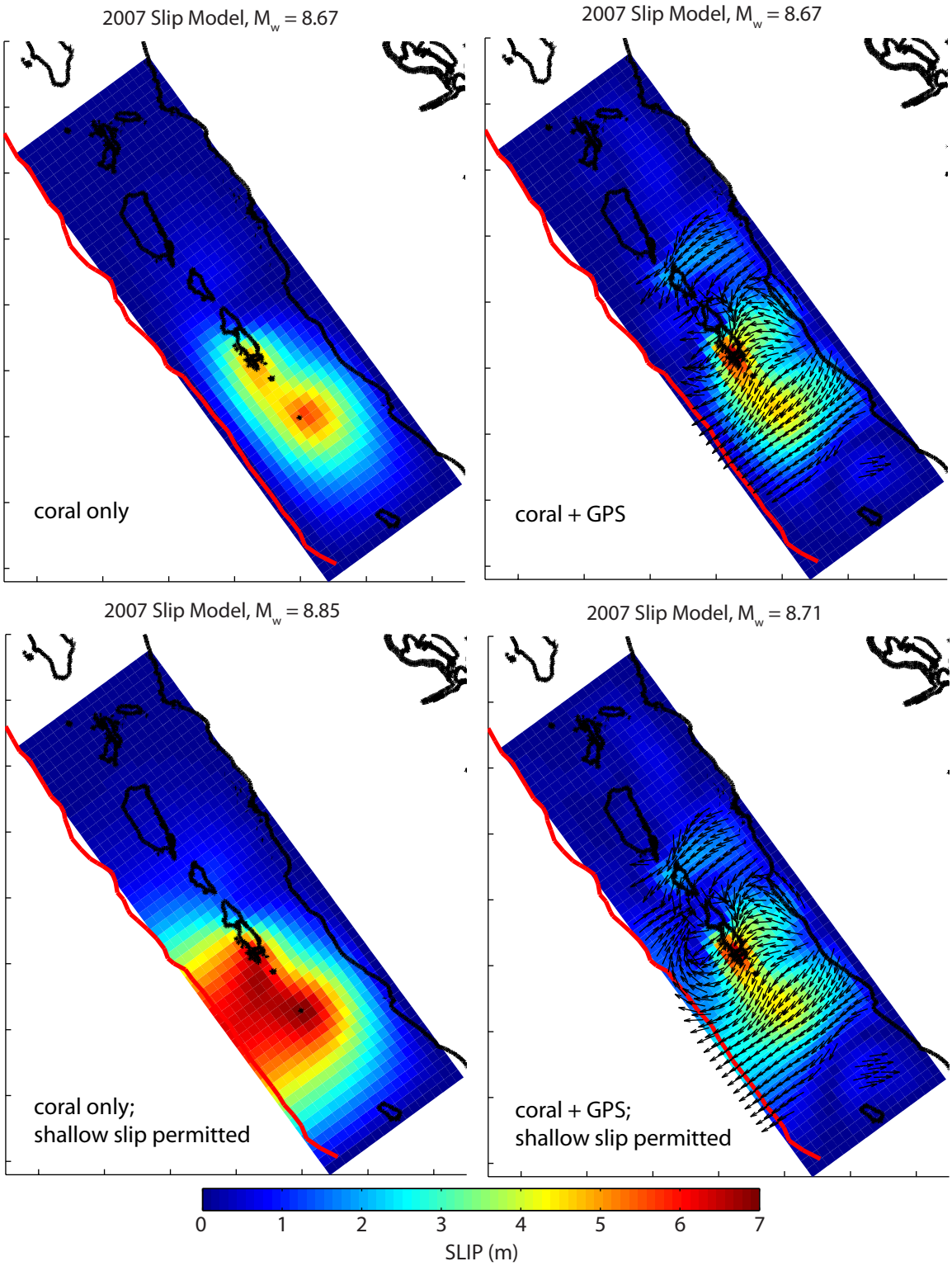

Figure S27. Comparison of models using only coral data or a combination of coral and GPS data for the 2007 earthquakes (data from *Konca et al.* [2008]). The coral-only models have a fixed dip-slip rake whereas the combined models have an unconstrained rake. With a zero-slip boundary condition at the trench, there is little difference between the models with and without GPS data. Neither dataset provides much constraint on shallow slip if it is permitted.

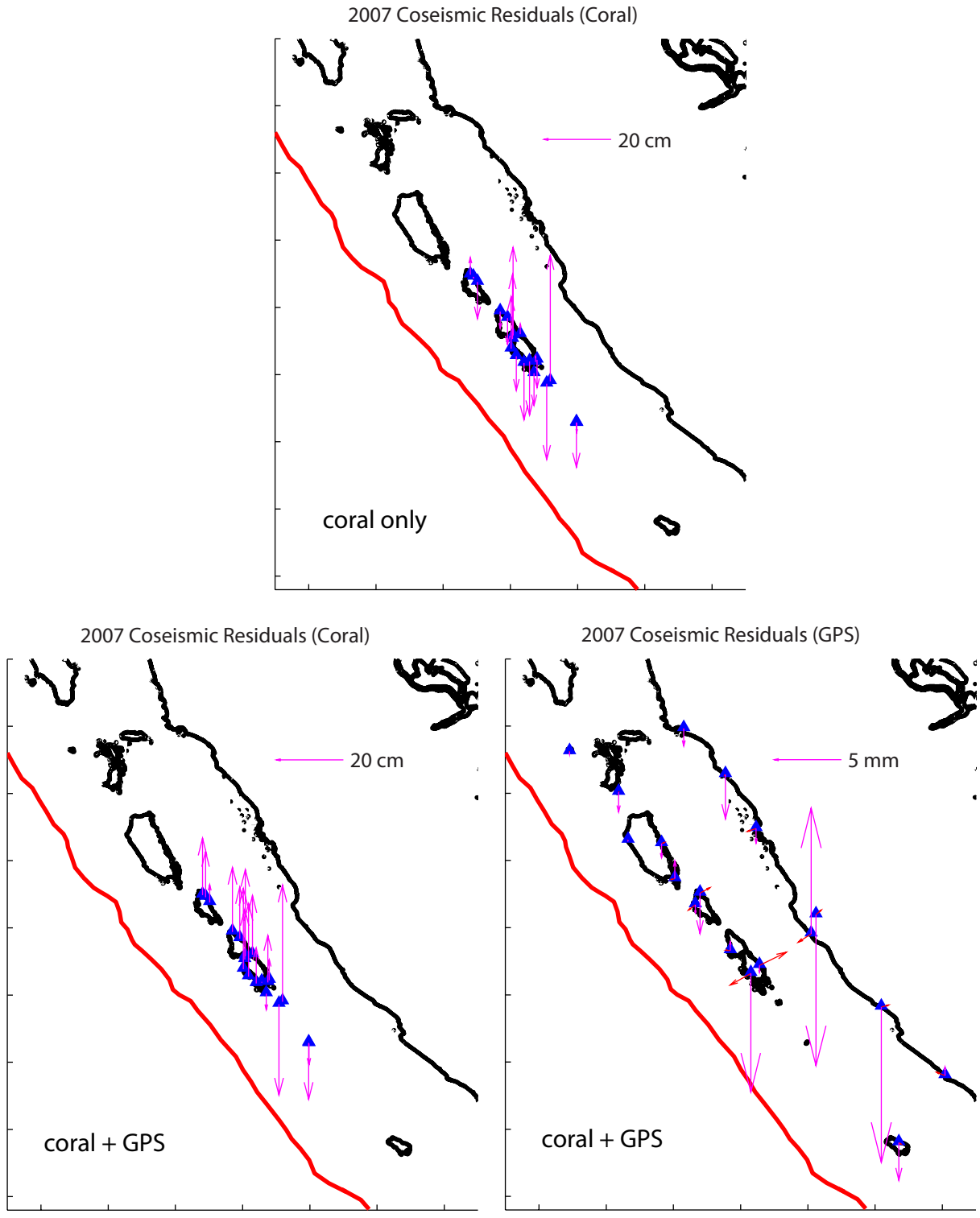

Figure S28. Residual vectors for the 2007 coseismic models. Pink arrows show vertical residuals and red arrows show horizontal residuals.

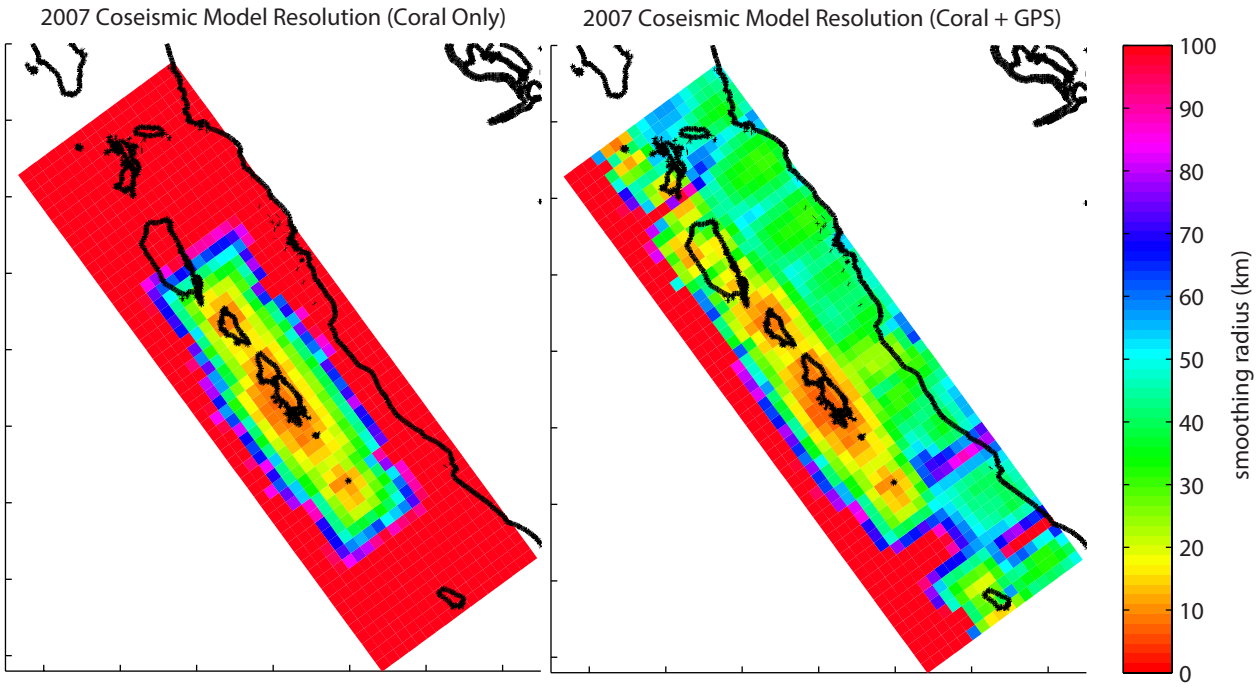

Figure S29. Comparison of model resolution using only coral data or a combination of coral and GPS data for the 2007 earthquakes. Based on coral data alone, the megathrust is essentially unresolved near the trench and below 45 km depth. GPS stations located along the Sumatran coast provide better resolution of the deep megathrust, but there is no improvement of resolution for the shallow megathrust.

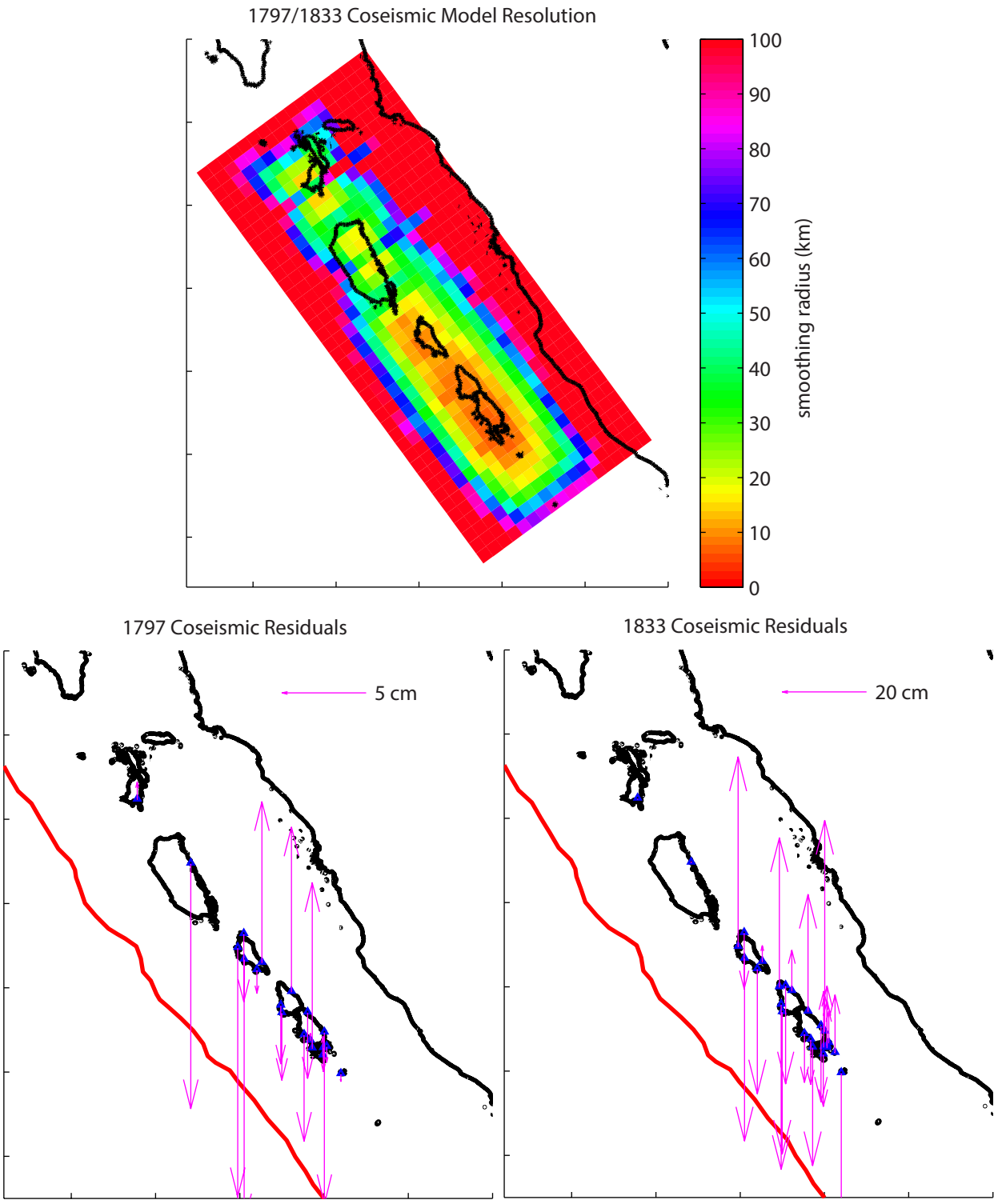

Figure S30. Resolution of the fault plane (in terms of smoothing distance) and residuals for the coseismic models. As we would expect, the shallow and deep parts of the megathrust are very poorly resolved. The fit to the 1797 uplift data is very good, within the data uncertainty virtually everywhere. The residuals for 1833 are much larger, but the fit is still acceptable since the uncertainties for 1833 uplift data are much larger than for 1797 (see Table 2).

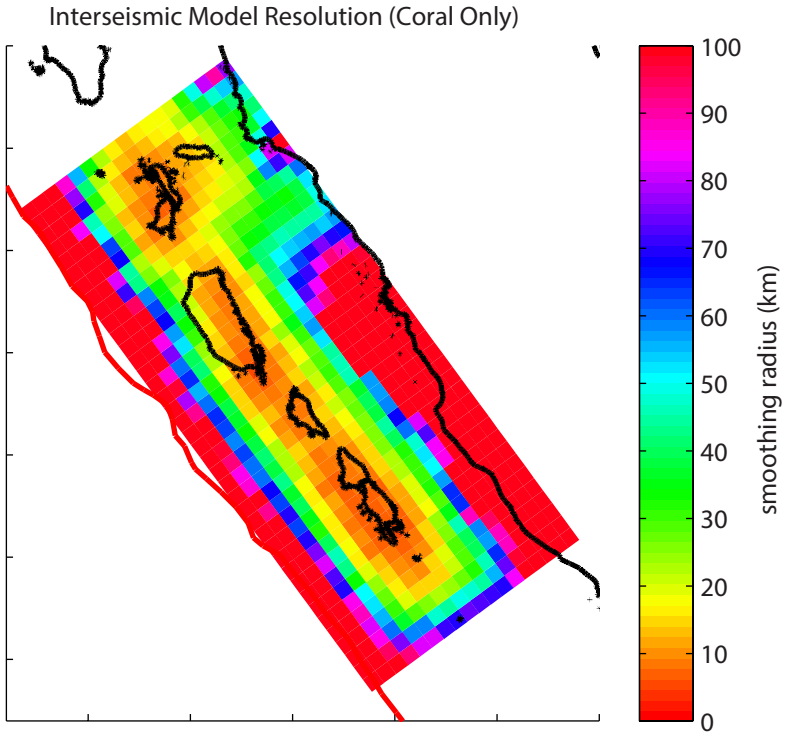

Figure S31. Resolution for coral-based interseismic models. The inclusion of synthetic data provides the same spatial distribution of sites for all these models.

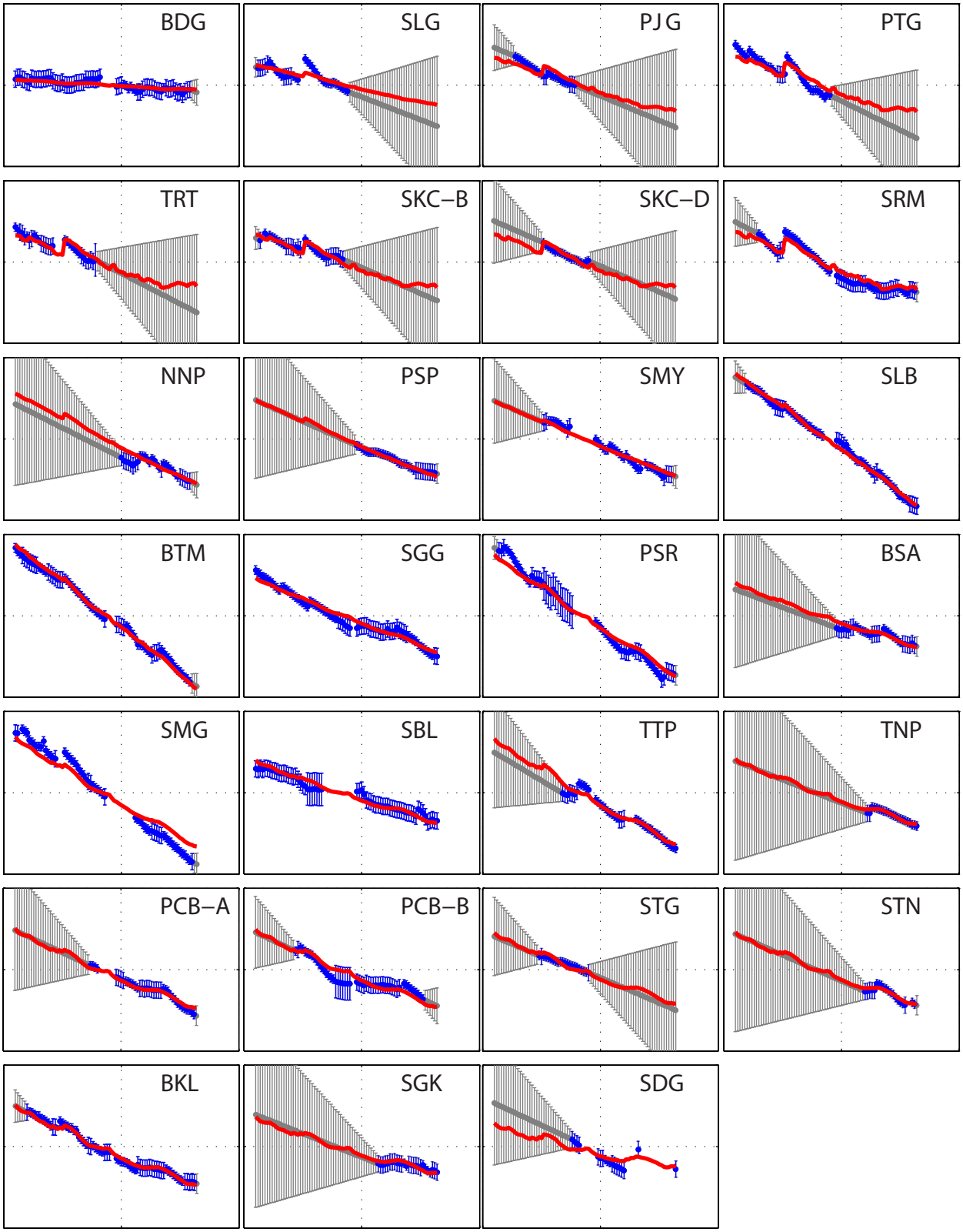

Figure S32. Coral data time series (blue) with synthetic supplementation (gray) and model (red) for interseismic deformation during the 1755–1833 period. All plots span 1750–1850 temporally (on the horizontal axis) and 1 meter vertically.

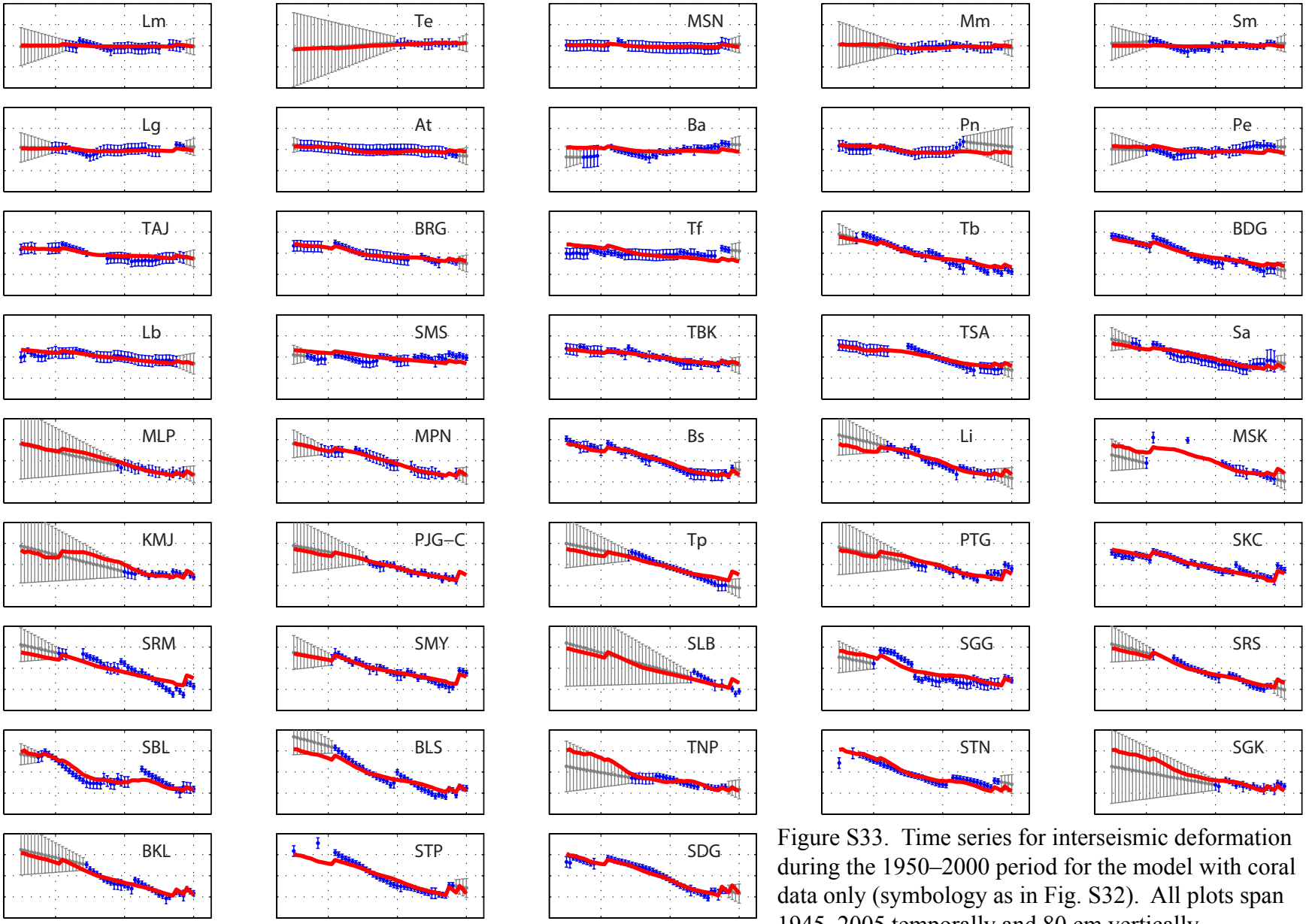

Figure S33. Time series for interseismic deformation during the 1950–2000 period for the model with coral data only (symbology as in Fig. S32). All plots span 1945–2005 temporally and 80 cm vertically.

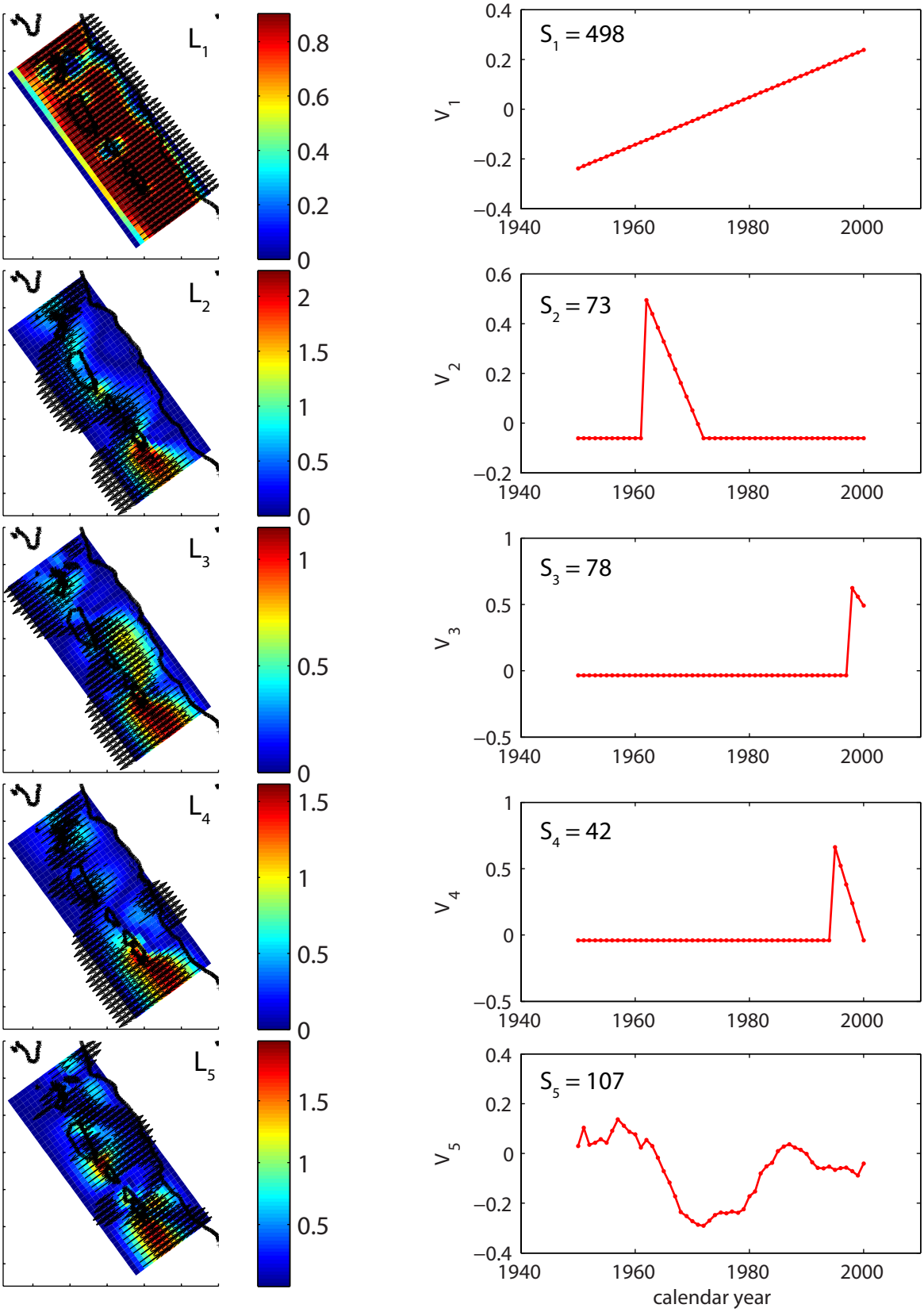

Figure S34. Spatial (L) and temporal (V) eigenvectors for the five-component 1950–2000 interseismic deformation model including coral and GPS data.

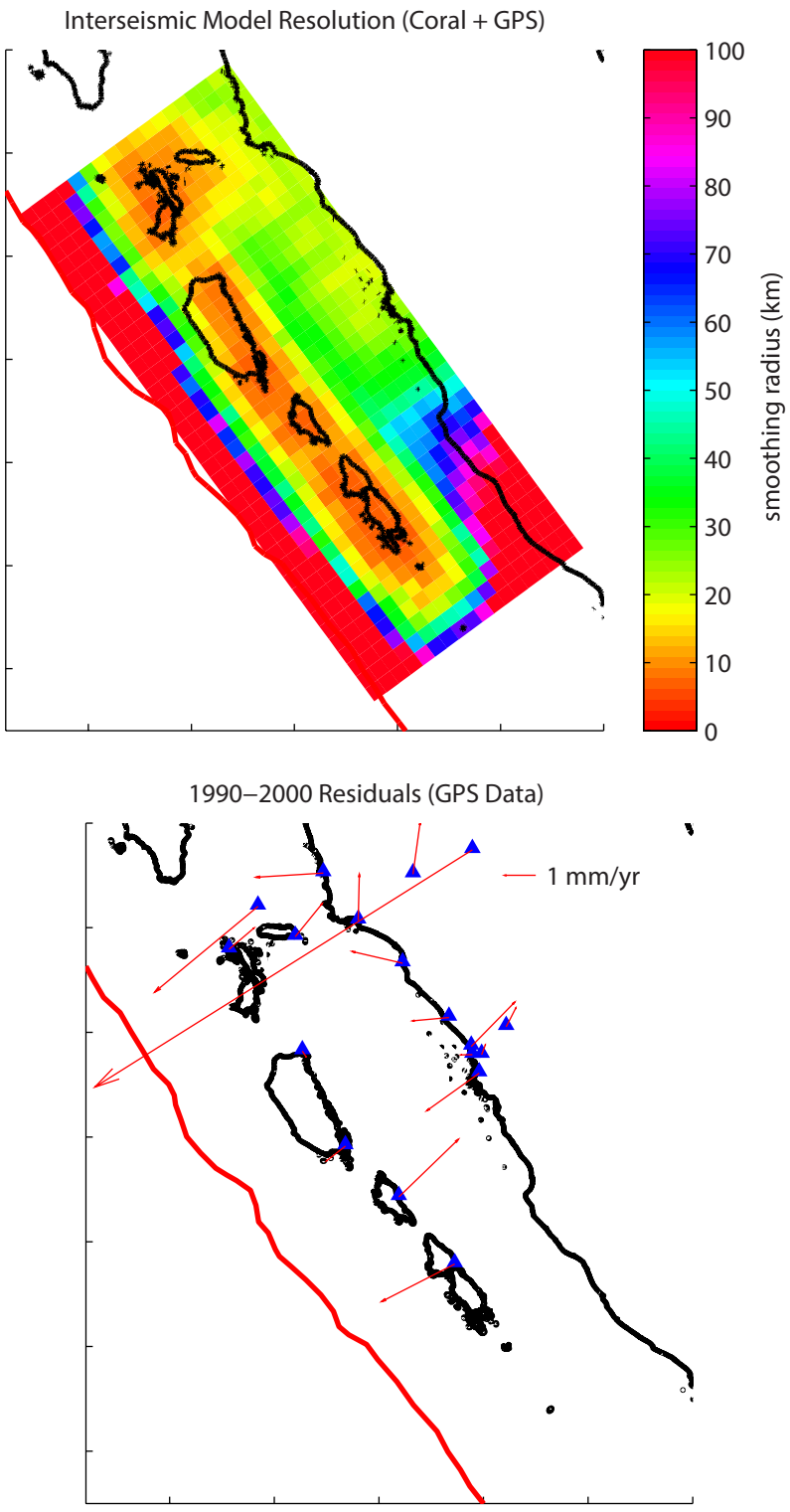

Figure S35. Model resolution and residuals for the combined coral + GPS interseismic model covering 1950–2000. The station with the anomalously large residual was measured over only two years, had a large uncertainty, and is farthest from the modelled fault plane. Other residuals are generally comparable to the ~2 mm/yr data uncertainties.

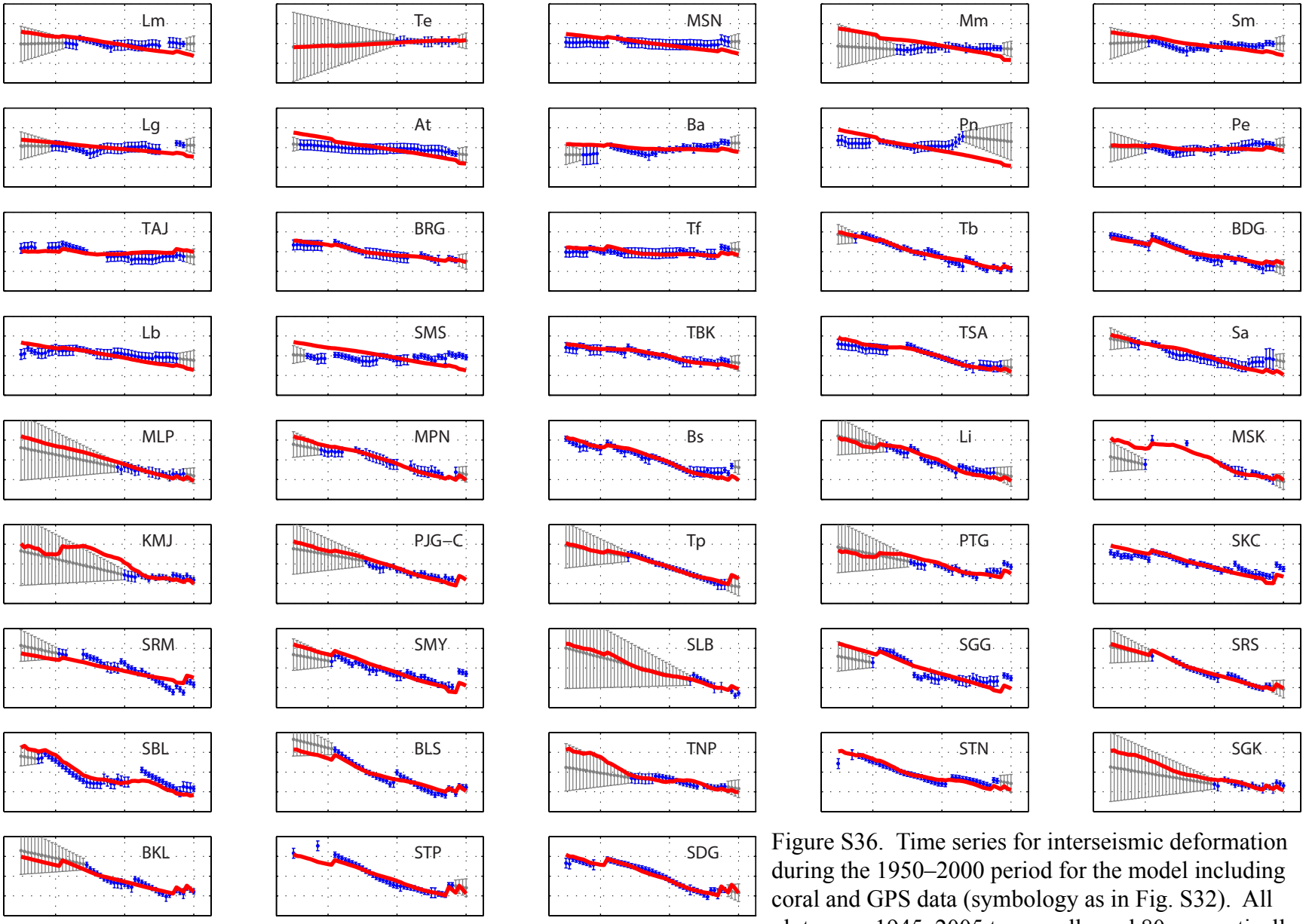

Figure S36. Time series for interseismic deformation during the 1950–2000 period for the model including coral and GPS data (symbology as in Fig. S32). All plots span 1945–2005 temporally and 80 cm vertically.

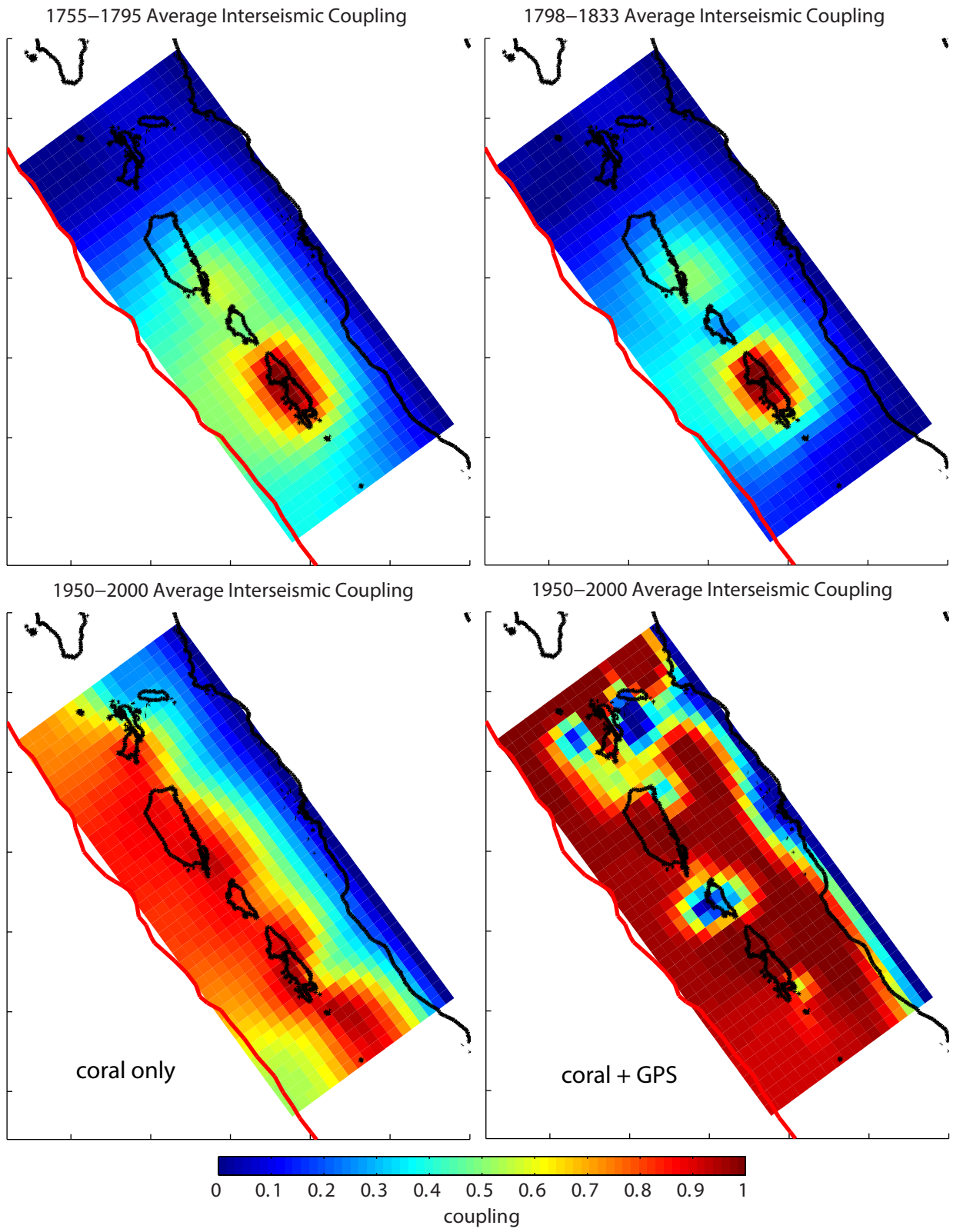

Figure S37. Interseismic coupling models unconstrained at the trench. As the shallow portion of the megathrust is very poorly resolved, these models fit the data equally as well as their counterparts with the updip edges constrained.

Table S1. Uranium and thorium isotopic compositions and ^{230}Th ages of coral subsamples by MC-ICPMS with dates A.D.

Subsample	^{238}U ppb	^{232}Th ppt	δ^{234}U measured[a]	[^{230}Th/^{238}U] activity[c]	[^{230}Th/^{232}Th] ppm[d]	Age uncorrected	Age corrected [c,e]	$\delta^{234}U_{initial}$ corrected[b]	$^{230}Th/^{232}Th_{initial}$ ppm[f]	Calendar Year A.D.[h]
PJG12-C3-1	1776.7 ± 1.6	129.8 ± 9.0	146.6 ± 1.6	0.002357 ± 0.000026	533 ± 37	224.7 ± 2.5	221.9 ± 3.7	146.7 ± 1.6		1790.1 ± 3.7
PJG12-C4-1	1711.0 ± 1.3	2345 ± 11	144.9 ± 1.7	0.004684 ± 0.000056	56.43 ± 0.73	447.6 ± 5.4	396 ± 52	145.0 ± 1.7		1616 ± 52
PJG12-C4-2	2274.1 ± 2.2	4568 ± 13	143.8 ± 1.5	0.005383 ± 0.000060	44.25 ± 0.50	515.1 ± 5.8	440 ± 76	143.9 ± 1.5		1573 ± 76
NPK10-A1-1-1	2190.9 ± 5.7	3816 ± 14	148.6 ± 3.1	0.002847 ± 0.000066	26.99 ± 0.63	271.0 ± 6.3				
NPK10-A1-1-2	2207.0 ± 2.3	5087 ± 12	147.0 ± 1.6	0.002847 ± 0.000073	20.39 ± 0.53	271.4 ± 7.0				
NPK10-A1-1-3	2184.5 ± 2.1	3647 ± 11	146.6 ± 1.5	0.002855 ± 0.000074	28.23 ± 0.74	272.2 ± 7.1				
NPK10-A1-1-4	2232.5 ± 3.9	3649 ± 10	146.4 ± 2.5	0.002817 ± 0.000064	28.46 ± 0.65	268.7 ± 6.2	267 ± 23	146.0 ± 6.2	0.3 ± 2.1	1744 ± 23
NPK10-A1-2	2033.9 ± 5.2	2250 ± 15	149.1 ± 3.6	0.003299 ± 0.000089	49.2 ± 1.4	313.9 ± 8.5	273 ± 42	149.2 ± 3.6		1739 ± 42
NPK10-A1-3	1447.2 ± 1.3	2274 ± 11	149.5 ± 1.6	0.003263 ± 0.000060	34.28 ± 0.65	310.4 ± 5.7	252 ± 59	149.7 ± 1.6		1760 ± 59
NPK10-A1-4	2255.4 ± 2.3	2811 ± 12	145.6 ± 1.6	0.002902 ± 0.000038	38.44 ± 0.53	276.9 ± 3.7	230 ± 47	145.7 ± 1.6		1783 ± 47
TRT10-A1-1	2351.3 ± 6.4	6636 ± 24	147.6 ± 2.9	0.003355 ± 0.000079	19.63 ± 0.46	320 ± 7.6	214 ± 106	147.7 ± 2.9		1796 ± 106
TRT10-A1-2	2258.9 ± 4.1	10587 ± 27	144.9 ± 2.4	0.00441 ± 0.00010	15.53 ± 0.35	421 ± 10				
TRT10-A1-2	2301.7 ± 3.3	8673 ± 21	147.0 ± 2.1	0.00398 ± 0.00011	17.43 ± 0.46	379 ± 10				
TRT10-A1-2	2333.5 ± 1.8	7458 ± 35	145.1 ± 1.6	0.003811 ± 0.000079	19.69 ± 0.42	364.0 ± 7.6				
TRT10-A1-2	2303.8 ± 2.1	7816 ± 20	145.3 ± 1.5	0.003754 ± 0.000075	18.27 ± 0.37	358.5 ± 7.2	224 ± 62	145 ± 15	7.2 ± 2.9	1788 ± 62
TRT10-A1-4	2172.4 ± 1.8	3106 ± 13	146.1 ± 1.8	0.003062 ± 0.000050	35.36 ± 0.60	292.1 ± 4.8	238 ± 54	146.2 ± 1.8		1774 ± 54
SKC08-D1	2239.5 ± 2.5	72.1 ± 4.1	146.1 ± 2.1	0.002293 ± 0.000034	1177 ± 68	218.7 ± 3.3	217.5 ± 3.5	146.2 ± 2.1		1790.5 ± 3.5
NNP10-A1-1-1	2460.4 ± 9.4	5275 ± 22	147.0 ± 4.4	0.003079 ± 0.000075	23.71 ± 0.58	293.5 ± 7.3				
NNP10-A1-1-2	2359.4 ± 4.1	4380 ± 13	149.0 ± 2.4	0.002883 ± 0.000062	25.64 ± 0.56	274.3 ± 5.9				
NNP10-A1-1-3	2452.3 ± 4.1	5712 ± 15	146.6 ± 2.4	0.003138 ± 0.000068	22.25 ± 0.48	299.3 ± 6.5				
NNP10-A1-1-4	2420.4 ± 4.6	4517 ± 14	149.4 ± 2.6	0.002883 ± 0.000065	25.50 ± 0.58	274.2 ± 6.3	172 ± 32	160 ± 13	9.4 ± 2.7	1839 ± 32
NNP10-A2-1-1	2366.6 ± 2.6	3965 ± 16	145.0 ± 1.6	0.002821 ± 0.000071	27.80 ± 0.71	269.3 ± 6.8				
NNP10-A2-1-2	2239.8 ± 2.3	5270 ± 13	143.2 ± 1.7	0.003030 ± 0.000073	21.26 ± 0.52	289.8 ± 7.0				
NNP10-A2-1-3	2272.4 ± 2.1	6062 ± 14	144.8 ± 1.6	0.003218 ± 0.000080	19.92 ± 0.50	307.4 ± 7.7				
NNP10-A2-1-4	2136.3 ± 2.2	5406 ± 13	145.9 ± 1.9	0.003120 ± 0.000081	20.35 ± 0.53	297.7 ± 7.8	208 ± 21	145.0 ± 5.7	6.2 ± 3.0	1803 ± 21
NNP10-A3-1	2132.8 ± 4.8	1765.3 ± 7.1	145.5 ± 2.4	0.002305 ± 0.000053	46.0 ± 1.1	220.0 ± 5.0	189 ± 31	145.6 ± 2.4		1821 ± 31
PSP08-A2-2	2020.2 ± 2.0	60.3 ± 6.2	147.6 ± 1.5	0.001874 ± 0.000052	1036 ± 110	178.4 ± 5.0	177.3 ± 5.1	147.7 ± 1.5		1831.7 ± 5.1
PSP08-A3-2	2180.2 ± 2.4	29.6 ± 6.3	148.9 ± 1.6	0.001949 ± 0.000050	2370 ± 509	185.4 ± 4.8	184.8 ± 4.8	149.0 ± 1.6		1824.2 ± 4.8
SSB10-A3-1	2447.4 ± 3.0	515.8 ± 7.2	142.7 ± 1.9	0.002697 ± 0.000050	211.3 ± 4.9	258.1 ± 4.8	250.1 ± 9.3	142.8 ± 1.9		1759.9 ± 9.3
SSB10-A3-2	2531.7 ± 2.0	1351.1 ± 7.4	146.9 ± 1.3	0.003080 ± 0.000031	95.3 ± 1.1	293.6 ± 2.9	274 ± 20	147.0 ± 1.3		1738 ± 20
BTM10-A1-1	2199.0 ± 3.6	505.3 ± 7.5	146.4 ± 2.0	0.002459 ± 0.000072	176.7 ± 5.8	234.5 ± 6.9	226 ± 11	146.5 ± 2.0		1784 ± 11
BTM10-A2-1	2008.4 ± 4.4	873.9 ± 6.6	147.1 ± 2.3	0.002150 ± 0.000058	81.6 ± 2.3	204.9 ± 5.6	189 ± 17	147.2 ± 2.3		1821 ± 17
BSA03A2-1b	2371.0 ± 3.0	2490.0 ± 8.0	148.5 ± 1.4	0.002640 ± 0.000030	41.5 ± 0.5	251.0 ± 3.0	212 ± 40	148.6 ± 1.4		1792 ± 40
SMG02-A2-1b	2131.8 ± 2.2	7129 ± 20	145.5 ± 1.8	0.003856 ± 0.000087	19.04 ± 0.43	368.2 ± 8.3				
SMG02-A2-1b	2239.7 ± 2.7	6242 ± 16	145.0 ± 1.8	0.003729 ± 0.000079	22.09 ± 0.47	356.2 ± 7.6				
SMG02-A2-1b	2358.6 ± 2.8	7737 ± 23	144.0 ± 1.9	0.003868 ± 0.000080	19.47 ± 0.40	369.8 ± 7.7				
SMG02-A2-1b	2107.5 ± 2.9	5342 ± 18	144.0 ± 2.1	0.003503 ± 0.000088	22.82 ± 0.58	334.9 ± 8.5	242 ± 35	142.2 ± 8.4	6.7 ± 2.1	1770 ± 35
PCB08-A1	1961.2 ± 1.4	56.6 ± 6.6	149.3 ± 1.3	0.001892 ± 0.000054	1082 ± 129	179.9 ± 5.2	178.8 ± 5.3	149.4 ± 1.3		1832.2 ± 5.3
PCB08-A2-1	2463.4 ± 1.6	461.6 ± 7.4	145.0 ± 1.3	0.001955 ± 0.000050	172.3 ± 5.2	186.6 ± 4.8	179.6 ± 8.5	145.0 ± 1.3		1828.4 ± 8.5
PCB08-B2-1	2319.6 ± 1.6	414.3 ± 7.1	145.6 ± 1.6	0.002066 ± 0.000051	191.0 ± 5.7	197.1 ± 4.8	190.4 ± 8.3	145.7 ± 1.6		1817.6 ± 8.3

Subsample	^{238}U ppb	^{232}Th ppt	$\delta^{234}U$ measured[a]	$[^{230}Th/^{238}U]$ activity[c]	$[^{230}Th/^{232}Th]$ ppm[d]	Age uncorrected	Age corrected [c,e]	$\delta^{234}U_{initial}$ corrected[b]	$^{230}Th/^{232}Th_{initial}$ ppm[f]	Calendar Year A.D.[h]
STG08-A1-1-1	2438.8 ± 2.0	31238 ± 114	144.5 ± 1.5	0.00464 ± 0.00019	5.98 ± 0.25	444 ± 18		144.6 ± 1.5		
STG08-A1-1-2	2451.8 ± 2.2	1797.4 ± 7.3	145.8 ± 1.6	0.002344 ± 0.000053	52.8 ± 1.2	223.6 ± 5.1		145.9 ± 1.6		
STG08-A1-1-3	2263.7 ± 2.0	2542.6 ± 7.8	148.3 ± 1.5	0.002392 ± 0.000062	35.17 ± 0.91	227.7 ± 5.9	205 ± 11	148.4 ± 1.5	3.2 ± 0.8	
STG08-A1-1-4	2356.3 ± 2.0	1370.8 ± 7.8	146.3 ± 1.5	0.002184 ± 0.000056	62.0 ± 1.6	208.2 ± 5.3	205 ± 29[g]	146.4 ± 1.5	3.2 ± 2.1[g]	1803 ± 29[g]
STG08-A1-2	2020.8 ± 1.6	1408.2 ± 5.9	145.4 ± 1.4	0.002972 ± 0.000028	70.43 ± 0.72	283.7 ± 2.7	258 ± 26	145.5 ± 1.4		1754 ± 26
STG08-A2	2015.7 ± 2.2	31.7 ± 3.6	147.6 ± 1.9	0.002329 ± 0.000039	2449 ± 281	221.9 ± 3.8	221.3 ± 3.8	147.7 ± 1.9		1786.7 ± 3.8
SGK10-A2-1	2417.3 ± 3.7	31.0 ± 6.2	147.7 ± 1.9	0.001860 ± 0.000047	2397 ± 487	177.1 ± 4.5	176.6 ± 4.5	147.7 ± 1.9		1833.4 ± 4.5
SDG10-A3-1	2477.2 ± 7.5	88.2 ± 5.8	148.9 ± 4.1	0.002060 ± 0.000049	956 ± 66	195.9 ± 4.7	194.6 ± 4.9	149.0 ± 4.1		1815.4 ± 4.9

Analytical errors are 2σ of the mean. Alternating gray and white shading groups analyses of single annual band samples.

[a] $\delta^{234}U = ([^{234}U/^{238}U]_{activity} - 1) \times 1000$.

[b] $\delta^{234}U_{initial}$ corrected was calculated based on ^{230}Th age (T), i.e., $\delta^{234}U_{initial} = \delta^{234}U_{measured} \; X \; e^{\lambda_{234} * T}$, and T is corrected age.

[c] $[^{230}Th/^{238}U]_{activity} = 1 - e^{-\lambda_{230} T} + (\delta^{234}U_{measured}/1000)[\lambda_{230}/(\lambda_{230} - \lambda_{234})](1 - e^{-(\lambda_{230} - \lambda_{234}) T})$, where T is the age.

Decay constants are 9.1577×10^{-6} yr^{-1} for ^{230}Th, 2.8263×10^{-6} yr^{-1} for ^{234}U [*Cheng et al.*, 2000], and 1.55125×10^{-10} yr^{-1} for ^{238}U [*Jaffey et al.*, 1971].

[d] The degree of detrital ^{230}Th contamination is indicated by the $[^{230}Th/^{232}Th]$ atomic ratio instead of the activity ratio.

[e] Age corrections were calculated using an estimated atomic $^{230}Th/^{232}Th$ ratio of 6.5 ± 6.5 ppm [*Zachariasen et al.*, 1999].

[f] For certain samples, more precise ages, $\delta^{234}U_{initial}$, and $^{230}Th/^{232}Th_{initial}$ values were derived from isochron techniques using an Excel macro, *Isoplot* 3.00 [*Ludwig and Titterington*, 1994; *Ludwig*, 2003].

[g] For isochron regressions with a p-value < 0.05, we increase the uncertainty of both the $^{230}Th/^{232}Th_{initial}$ and the age by a factor of the square root of the mean square of weighted deviates (MSWD), as suggested by *Ludwig* [200

[h] Calculated by subtracting the corrected sample age from the year of chemical analysis.

References

Cheng, H., R. L. Edwards, J. Hoff, C. D. Gallup, D. A. Richards, and Y. Asmerom (2000), The half-lives of uranium-234 and thorium-230, *Chemical Geology*, *169*, 17-33.

Jaffey, A. H., K. F. Flynn, L. E. Glendenin, W. C. Bentley, and A. M. Essling (1971), Precision measurements of half-lives and specific activities of ^{235}U and ^{238}U, *Physical Review C*, *4*, 1889-1906.

Ludwig, K. R. (2003), Mathematical–statistical treatment of data and errors for $^{230}Th/U$ geochronology, *Reviews in Mineralogy and Geochemistry*, *52* (1), 631-656.

Ludwig, K. R., and D. M. Titterington (1994), Calculation of $^{230}Th/U$ isochrons, ages, and errors, *Geochim. Cosmochim. Acta*, *58* (22), 5031-5042.

Zachariasen, J., K. Sieh, F. W. Taylor, R. L. Edwards, and W. S. Hantoro (1999), Submergence and uplift associated with the giant 1833 Sumatran subduction earthquake: Evidence from coral microatolls, *J. Geophys. Res.*, *104* (B1), 895-919.